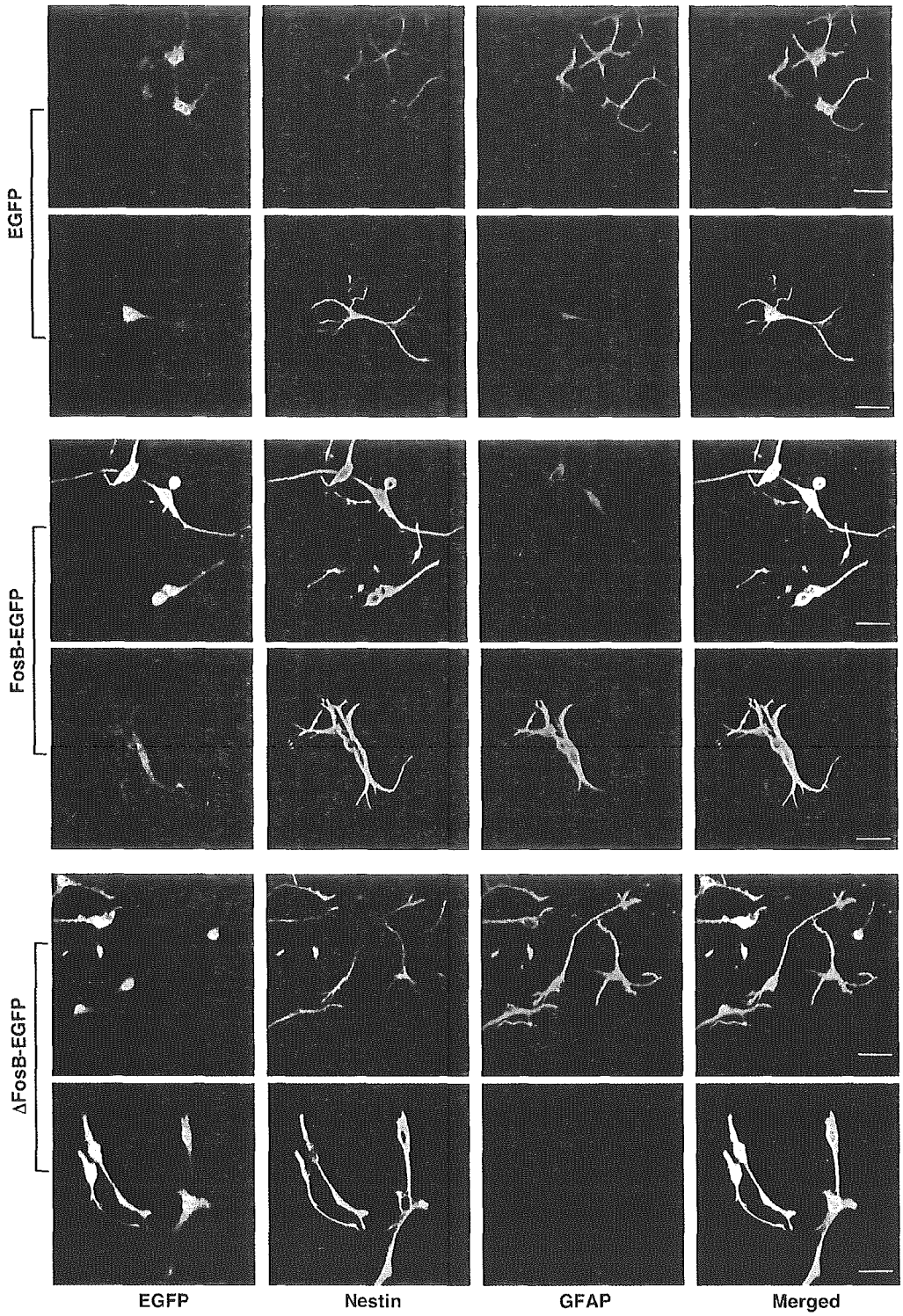

Figure 9 Phenotypical changes of the rat embryonic cortical cells induced by FosB or ΔFosB expression. Rat embryonic cortical cells were infected with each recombinant adenovirus encoding EGFP alone, FosB-EGFP and ΔFosB-EGFP, as indicated on the left side, and then were cultured for 4 days in the presence of B27 supplement. At 2 days after the culture medium was changed to a Neurobasal medium lacking B27 supplement, the cells were fixed and subjected to immunofluorescence microscopy. Green: EGFP fluorescence; red: nestin immunofluorescence; blue: GFAP immunofluorescence; merged: the merged view of the three fluorescences. Scale bars, 50 μm

Table 3 Expression of nestin and GFAP in adenovirus-infected rat embryonic cortical cells

Adenovirus	Number of EGFP-positive cells			
	Nestin$^+$/GFAP$^+$	Nestin$^+$/GFAP$^-$	Nestin$^-$/GFAP$^+$	Nestin$^-$/GFAP$^-$
EGFP	15	5	2	1
FosB-EGFP	5	16	0	0
ΔFosB-EGFP	17	23	1	5

Rat embryonic cortical cells were infected with each recombinant adenovirus encoding EGFP alone, FosB-EGFP or ΔFosB-EGFP, and then were cultured for 4 days in the presence of B27 supplement. At 2 days after the culture medium was changed to a Neurobasal medium lacking B27 supplement, the cells were fixed and subjected to immunofluorescence microscopy for nestin and GFAP. The number of cells in areas of the same size was counted

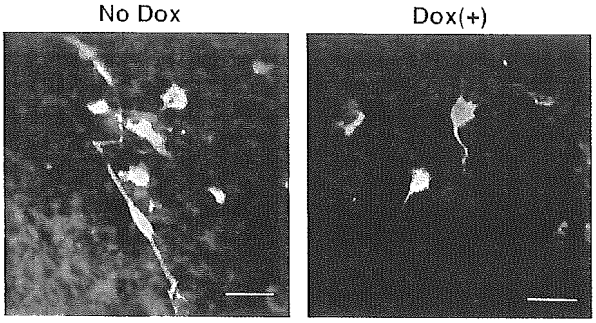

Figure 10 Expression of neural marker in rat embryonic cortical cells after the expression of ΔFosB was shut-off. Rat embryonic cortical cells infected with the recombinant adenovirus coding ΔFosB-EGFP were cultured for 2 days in the presence of B27 supplement, and then the cells were maintained in Neurobasal medium lacking B27 supplement for 13 days. Doxycycline (Dox (+), final 400 ng/ml) was added to half of the cultures, and the rest was maintained without doxycycline (No dox). After 4 days, the cells were fixed and subjected to immunofluorescence microscopy with anti-MAP2 antibody. Red: MAP2 immunofluorescence; green: EGFP fluorescence. The merged views are shown. In parentheses, total numbers of MAP2-positive and EGFP-positive cells observed in the experiment are shown (MAP2/EGFP). Scale bars, 50 μm

cells expressed EGFP. The cells infected with adenovirus coding FosB-EGFP exhibited immunoreactivities both for anti-FosB(102) and anti-FosB(C), while those with adenovirus coding ΔFosB-EGFP exhibited immunoreactivity only for anti-FosB(102) but not anti-FosB(C), and neither immunoreactivity was detected in those with adenovirus coding EGFP alone (Figure 11). As a result, we reproduced the specific expression of ΔFosB in cells within the ventricle wall, as we observed in the rats after ischemic insult.

We next examined the expression of nestin and GFAP in the adenovirus-infected cells, as shown in Figure 12. The nestin expression level was low in normal ependymal or subependymal cells and in those infected with adenovirus coding EGFP alone. However, the nestin immunoreactivity in cells expressing FosB and ΔFosB increased significantly in comparison to those infected with adenovirus coding EGFP alone or adjacent EGFP-negative cells. Interestingly, the cells expressing ΔFosB maintained a nonpolar shape, while those expressing FosB tended to show a polar shape. GFAP immunoreactivity in cells expressing FosB or ΔFosB was not elevated in comparison to nestin; however, the cells neighboring the subependymal layer showed an increased GFAP immunoreactivity in comparison to the control. Again, these observations may suggest that some secretary factor(s) from FosB- or ΔFosB-expressing cells may promote the proliferation of neuronal precursor cells.

As seen in the embryonic cortical cell culture, the expression of ΔFosB in cells within the ventricle wall also increased the expression of nestin but not that of GFAP.

Discussion

Our major conclusion in the present study is that the expression of ΔFosB was induced in cells within the ventricle wall as well as in the hippocampus prior to neurogenesis after transient forebrain ischemia; that the expression of ΔFosB in cells within the ventricle wall resulted in an elevated expression of nestin; that ΔFosB triggered the proliferation of neuronal progenitor-like cells; and that the decline in ΔFosB expression plays important roles in promoting the maturation of neurons.

In the brain of adult rats, the expression of *fosB* gene products, FosB and ΔFosB, is very low; however, various types of brain insult, such as transient forebrain ischemia or excitotoxicity, result in a significant induction of their expression in the hippocampus prior to neuronal loss, as well as other AP-1 proteins such as c-Fos and c-Jun or JunB.[13] Among them, the induction of c-Fos expression is very rapid and transient and its level returns to basal level within a couple of hours after transient forebrain ischemia, while the levels of FosB and ΔFosB or c-Jun expression persistently elevated 2–48 h after the insult. The level of JunB expression is slowly elevated 12–24 h after transient forebrain ischemia, while the level of JunD expression is almost constant either with or without the insult. Since the phosphorylation of c-Jun by Jun amino-terminal kinases (JNK) such as JNK3 plays a key role in apoptosis or neurodegeneration, the induced expression of these AP-1 proteins after transient forebrain ischemia has been implicated in the neuronal loss caused by insult.[28,29]

In the present study, we found the expression of ΔFosB but not that of FosB to be selectively induced in cells within the ventricle wall as well as in the hippocampus 2 days after the transient forebrain ischemia, and that these cells also exhibited a markedly elevated expression of nestin, which is a class IV intermediate filament protein and a marker for neuronal precursor cells in the adult brain.[30,31] At 7 days after ischemia, although the ΔFosB expression was as low as at the basal level, the nestin-positive cells were enriched in the outer

boundary zones to the ischemic core in the cerebral cortex as well as in the CA1 and DG subfields of the hippocampus, where BrdU-positive cells were also enriched. We further observed an increased expression of galectin-1 in the nestin-positive cells in the hippocampus but not within the ventricle wall, at 7 days after ischemia. Since ΔFosB as well as FosB increased the expression of both galectin-1 and nestin in the embryonic cortical cells, ΔFosB induced in the hippocampus after ischemia is therefore likely responsible for the increased expression of galectin-1, and we are now confirming this possibility using *fosB*-null mice.

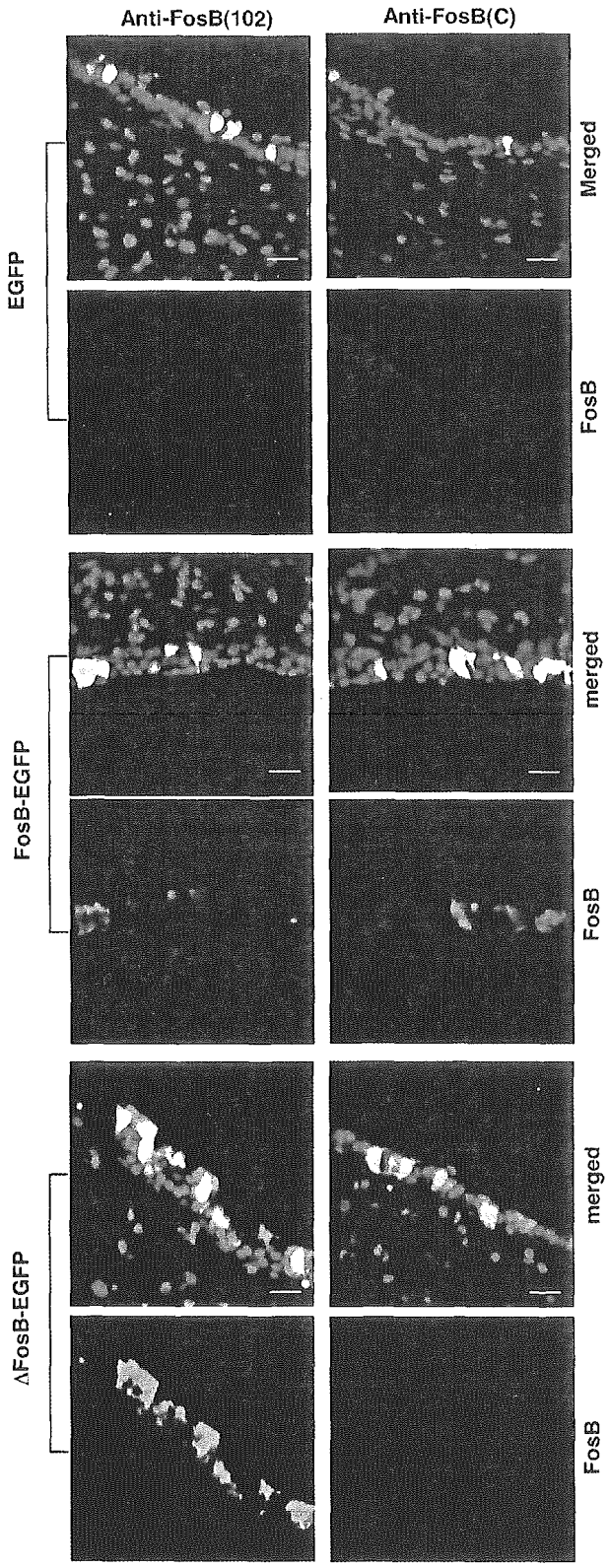

We previously demonstrated that an artificial expression of ΔFosB, and to a lesser extent FosB, triggers DNA replication and cell division in quiescent fibroblast cells in the absence of serum.[18–21] Furthermore, neurogenesis in the adult mammalian brain has been proven to occur in the SVZ and DG of the hippocampus, and it is likely to be promoted by stress such as ischemic insult.[14–17] Therefore, our observation strongly suggests that the ischemia-induced expression of ΔFosB in cells within the ventricle wall or neuronal precursor cells in DG promotes the proliferation or migration of such neuronal precursor cells to the damaged area in the brain to replace the damaged neurons. Furthermore, our data suggest that the decline in the ΔFosB expression following the proliferation is essential for maturation of neurons.

As we demonstrated in rat 1a cells, the adenovirus-mediated expression of ΔFosB, and to a lesser extent FosB, in rat embryonic cortical cells resulted in the selective proliferation of nestin-positive cells even after the withdrawal of B27 trophic support, which promotes the survival of primary neurons *in vitro*. The surviving cells, in the presence of ΔFosB or FosB, underwent DNA replication and mostly expressed nestin, while less than half of them expressed GFAP also. Some of the cells expressing ΔFosB or FosB, which dominantly expressed nestin over GFAP, were morphologically most likely radial glial cells, while those with dominant expression of GFAP were most likely astrocytes (Figure 9). The decline in ΔFosB expression in these cells converted some of them to MAP2-positive, thus suggesting that ΔFosB promotes the proliferation of neuronal precursor cells without their neuronal maturation, at least *in vitro*.

The injection of recombinant adenovirus into the ventricle of the rat brain revealed that the expression of ΔFosB in cells within the ventricle wall indeed increased nestin immunoreactivity, but not GFAP immunoreactivity, as we observed in both the rat brain after ischemic insult and adenovirus-infected cortical cell culture, thus indicating that ΔFosB may stimulate proliferation of neuronal precursor cells, and as a result, the expression of nestin is likely to be upregulated. It has recently been shown that two distinct subpopulations (type I and type II) of nestin-positive cells are present in the adult mouse DG.[31] Type I cells have a lower input resistance

Figure 11 Adenovirus-mediated expression of FosB and ΔFosB in cells within the ventricle wall of the rat brain. The brain sections were prepared from the rats 54 h after the adenovirus injection, and then were subjected to confocal laser-scanning microscopy after reaction with anti-FosB(102) or anti-FosB(C) with Alexa-labeled second antibody (red). The nuclei were counterstained with DAPI (blue). Infected cells were identified by EGFP fluorescence (green). Merged: the merged images. In the sections from the brain infected with adenovirus encoding EGFP alone (EGFP) or ΔFosB-EGFP (ΔFosB-EGFP), EGFP-positive cells were mostly detected in the third ventricle wall, while in the sections from the brain infected with adenovirus encoding FosB-EGFP (FosB-EGFP), EGFP-positive cells were mostly detected in the LV wall. Scale bars: 25 μm

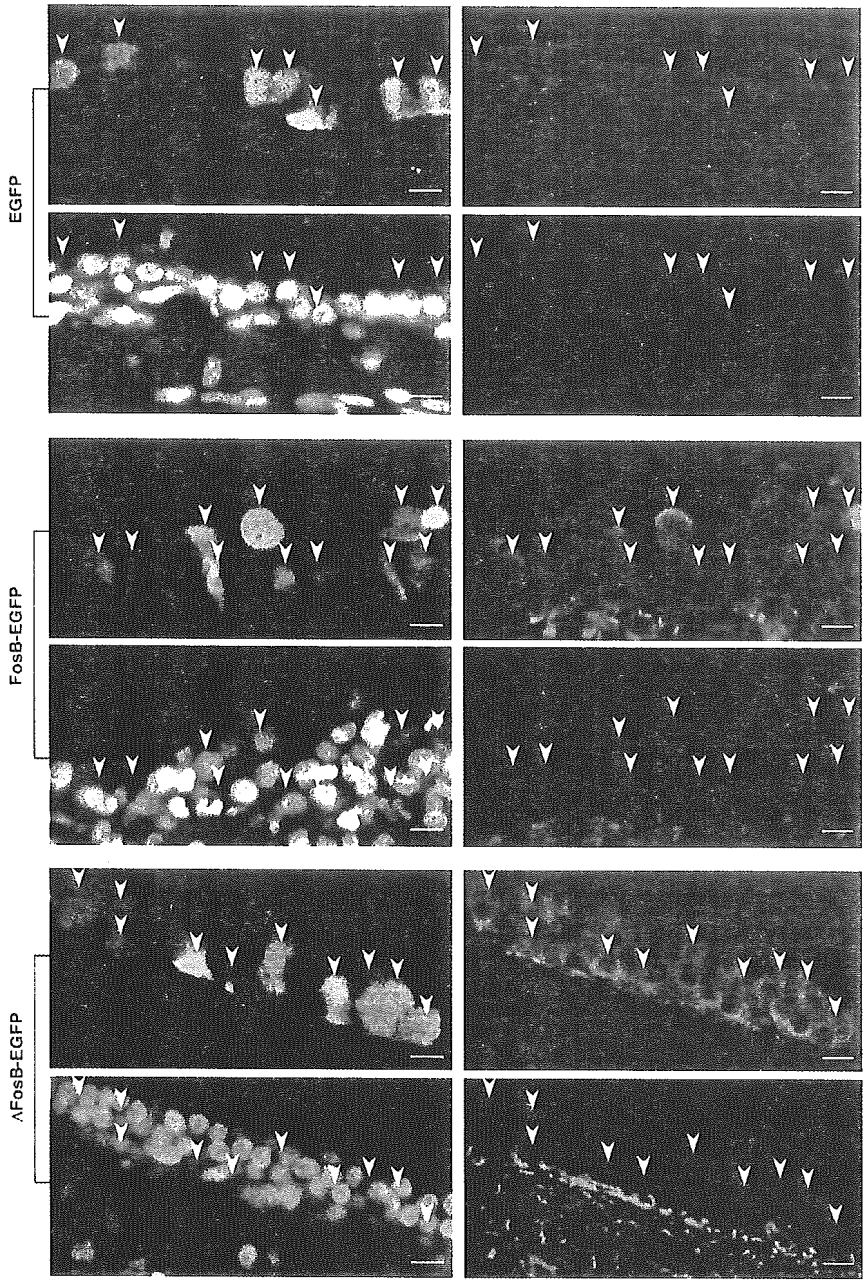

Figure 12 ΔFosB expression in cells within the ventricle wall induces nestin expression. The brain sections were prepared as described in Figure 11, and subjected to laser-scaning confocal microscopy after reaction with anti-nestin (red) and anti-GFAP (blue) with proper Alexa-labeled second antibodies, and infected cells (arrowheads) were identified by EGFP fluorescence (green). The nuclei were counterstained with DAPI (yellow). In the sections from the brain infected with adenovirus encoding EGFP alone (EGFP), both nestin and GFAP were barely detectable. In the brain sections infected with adenovirus encoding ΔFosB-EGFP (ΔFosB-EGFP) or FosB-EGFP (FosB-EGFP), nestin immunoreactivity mostly increased in the EGFP-positive cells, while an increased GFAP immunoreactivity was seen in an adjacent layer to the EGFP-positive cell layer. Scale bars: 10 μm

value, and their radial processes are GFAP-positive, whereas type II cells have a higher input resistance value and are GFAP-negative. It is suggested that there is a rapid and dynamic cell conversion of nestin-positive progenitors, from type I to type II, at an early stage of adult neurogenesis. It has recently been reported that GFAP-expressing progenitors are a principal source of constitutive neurogenesis in adult rodent forebrain,[32] thus suggesting that ΔFosB may promote the proliferation of a subset of progenitor cells, such as type II nestin-positive/GFAP-negative cells.

At 7 days after transient forebrain ischemia, the levels of FosB or ΔFosB expression in the brain returned to almost basal levels, and many newly generated cells most likely migrated to damaged places (Figure 3). It was shown that

newly generated neurons appear to replace the damaged neurons several weeks after the initial insult; thus, the decline in ΔFosB expression may be a prerequisite for such migration and/or maturation of newly generated neurons. Adenovirus-mediated expression of ΔFosB in cells within the ventricle wall resulted in an elevated expression of nestin, but not their proliferation or migration, thus suggesting that other factors that can be induced in the brain due to some stimulation or stress might be required for their proliferation and migration.

The adenovirus-mediated expression of FosB or ΔFosB resulted in their preferential localization in the cytoplasm of both rat 1a and embryonic cortical cells, thus indicating that a large part of overexpressed FosB or ΔFosB remained in the cytoplasm. The expression of FosB or ΔFosB in the embryonic cortical cells resulted in an increased expression of each Jun protein, and JunD protein was preferentially detected in the nuclei among them (Figure 5). These results suggest that a part of overexpressed FosB or ΔFosB formed functional AP-1 heterodimers with JunD and to a lesser extent with c-Jun or JunB, as we previously demonstrated in the rat 1a embryonic fibroblasts.[18] However, we could not rule out the possibility that cytoplasmic FosB or ΔFosB may play some role in these cells.

Semiquantitative RT-PCR analyses showed that the expression of *Mmp3* gene, which is known to be upregulated by FosB but not ΔFosB in rat 1a cells as an AP-1-responsive gene,[18] was not detected in any of the embryonic cortical cells even with the expression of FosB. Furthermore, the expression of *Cdk5* and *GluR2* genes, which are known to be upregulated in the striatal neurons of ΔFosB-transgenic mice, was not altered in any of the embryonic cortical cells regardless of the FosB or ΔFosB expression, thus suggesting that in the embryonic cortical cells, neither FosB nor ΔFosB can alter the expression of known targets of FosB or ΔFosB in fibroblasts or neurons. However, we found that the expression of the *JunB* gene among the three *Jun* genes increased most remarkably in the embryonic cortical cells expressing FosB but not ΔFosB, thus suggesting that FosB or ΔFosB is involved in the regulation of a different set of genes in the embryonic cortical cells in comparison to those in fibroblasts or neurons. A functional analysis of FosB or ΔFosB on *JunB* expression may shed light on the mechanism of how FosB or ΔFosB regulates gene expression in the neuronal precursor cells.

Semiquantitative RT-PCR analyses also revealed that the increased expression of nestin and GFAP in the embryonic cortical cells by FosB or ΔFosB is partly due to the increased levels of their transcripts. It has been shown that the ectopic expression of ΔFosB in transgenic mice altered the gene expression profiles in neurons, and some were upregulated while others were downregulated.[10,11] Our data suggest that ΔFosB lacking the C-terminal transactivating domain in FosB can upregulate the expression of *Nestin* and *Gfap* genes in neuronal precursor cells, thus promoting their proliferation.

We recently identified galectin-1 to be a secretory factor whose expression is induced by ΔFosB in embryonic cell lines,[20–22] and we herein showed the expression of galectin-1 to be significantly upregulated in the embryonic cortical cells by either FosB or ΔFosB, as well as in the hippocampus after ischemia. Furthermore, our data also indicate that galectin-1, as a secretory factor from FosB- or ΔFosB-expressing cells, appears to promote the proliferation of embryonic cortical cells. We are now examining whether galectin-1 participates in such a proliferative response in the damaged brain.

It has been considered that efficient propagation of neuronal precursor cells *in vitro* is one of the most critical factors for stem cell therapy for neurodegenerative disorders. Our results strongly suggest that ΔFosB efficiently promotes the selective proliferation of neuronal precursors without their maturation even under a certain stressed condition, thus providing us with clues to develop new approaches to stem cell therapy.

Materials and Methods

Antibodies

The FosB(C) antibody was raised against amino acids 245–315 of the C-terminus of FosB.[5] Since the C-terminus is missing in ΔFosB, the FosB(C) antibody only recognizes FosB.[18] Rabbit polyclonal antibodies against c-Jun and JunB have been described previously.[33,34] For preparation of anti-JunD antibody, TrpE-JunD (1–92 aa) fusion protein was immunized to rabbits and antiserum was affinity purified as described previously.[5] The FosB(102) antibody (sc-48, sc-48G), and rabbit or goat polyclonal antibodies whose epitope was mapped within a common central domain (residues 75–150) of FosB and ΔFosB were products of Santa Cruz Biotechnology (Santa Cruz, CA, USA). Rabbit polyclonal antibodies to glial fibrillary acidic protein (GFAP) were purchased from DakoCytomation (Kyoto, Japan). Mouse monoclonal antibodies to GFAP (G-A-5), β-tubulin III (SDL.3D10) and MAP2 (HM-2) were products of Sigma (St. Louis, MO, USA). Mouse monoclonal antibody to nestin (Rat401) was obtained from BD Bioscience Pharmingen (San Diego, CA, USA), and mouse monoclonal antibody to BrdU (BMC9318) was obtained from Roche Diagnostics Japan (Tokyo, Japan). Alexa-labeled second antibodies were obtained from Invitrogen Japan (Tokyo, Japan). The rabbit polyclonal antibodies (anti-rhGal-1) against recombinant human galectin-1 have been described previously.[35]

Transient forebrain ischemia model

All animal experiments were conducted in accordance with the national prescribed guidelines, and ethical approval for the present studies was granted by the Animal Experiment Committee of Kyushu University. Transient forebrain ischemia was performed using published modifications[23] of the 2-VO method.[36] Briefly, male stroke-prone spontaneously hypertensive rats (SHRSP/Izm, Japan SLC, Hamamatsu, Japan) weighing 250–300 g and aged 13–15 weeks were anesthetized with halothane. Both common carotid arteries were exposed and separated, and then were loosely encircled with polyethylene tubes for later ligation. Forebrain ischemia was achieved by tightening polyethylene tubes for 20 min. The brain temperature, measured indirectly via a thermocouple probe placed in the temporalis muscle, was maintained at close to 37°C throughout the operations. To detect dividing cells in the brain, BrdU (50 mg/kg; Sigma) was given to rats by intraperitoneal injection once a day after the operation for 7 days.

Immunohistochemistry

Rats were deeply anesthetized with 1.5%. halothane, and perfused transcardially with 50 ml of heparinized saline (0.9%) followed by 150 ml of 0.1 M PBS containing 4% paraformaldehyde. The brains were fixed in 4% paraformaldehyde at 4°C for 12–24 h and embedded in paraffin. Coronal

sections (4 μm) were deparaffinized, pretreated in 3% hydrogen peroxide in methanol and subjected to immunohistochemistry with each antibody. Sections were processed using the Vectastain ABC or ABC-AP KITs (Vector laboratories, Burlingame, CA, USA) with a proper biotinylated secondary antibody, and peroxidase reaction product was detected using 3'3'-diaminobenzidine-tetrahydrochloride (Sigma), and alkaline phosphatase reaction product was detected with Vector Blue (Vector Laboratories). Digital images were acquired using Axioskop2 plus equipped with AxioCam (Carl Zeiss Japan, Tokyo).

Rat embryonic cortical cell primary culture

Cultures of embryonic cortical cells were prepared from embryonic day 18 Wister Kyoto (WKY) rats (Kyudo, Kumamoto, Japan), as described.[26] Cells were plated at an indicated density on polyethylenimine (PEI) (Sigma)-coated glass coverslips or 96-well plates in Neurobasal medium with B27 supplement (Invitrogen) containing penicillin/streptomycin (100 U/ml), 0.5 mM L-glutamine and 10 μM 2-mercaptoethanol. Cultures were maintained in a 95% room air and 5% CO_2 humidified atmosphere at 37°C. Rat embryonic cortical cells cultured on PEI-coated glass coverslips were fixed in 0.1 M PBS containing 4% paraformaldehyde for 15 min, and were processed for immunofluorescence microscopy.

Galectin-1 preparation

The recombinant mouse galectin-1α and galectin-1β were prepared as described previously.[22]

Adenovirus vector

Adenovirus vector expressing FosB or ΔFosB was constructed using Adeno-X Tet-Off Expression System 1, according to the user manual (PT3496-1, BD Biosciences Clontech, Palo Alto, CA, USA). Briefly, an *Eco*RI–*Bam*HI fragment containing the entire coding region of mouse FosB or ΔFosB was subcloned into pIRES2-EGFP vector (Clontech). An *Nhe*I–*Not*I fragment containing the entire coding region of mouse FosB or ΔFosB and an IRES followed by EGFP coding region was inserted into the *Xba*I–*Not*I sites of the pTRE-Shuttle vector. A fragment containing FosB or ΔFosB with EGFP placed under the control of Tet-responsive expression cassette was excised by I-*Ceu*I and PI-*Sce*I, and inserted into Adeno-X system 1 viral DNA, which is a derivative of a replication-incompetent (ΔE1/ΔE3) human adenoviral type 5 genome. *Pac*I-linearized recombinant Adeno-X viral DNA was transfected into HEK293 cells using Lipofectamine 2000 (Invitrogen, Japan) according to the manufacturer's instruction manual. Harvested recombinant adenovirus was propagated and titrated on HEK293 cells. The recombinant adenoviruses obtained were purified by Adeno-X Virus Purification Kits (Clontech). The titer of each viral stock was $\sim 1.85 \times 10^9$ PFU/ml for Adeno-X:TRE-FosB-EGFP (FosB-EGFP), $\sim 2.62 \times 10^9$ PFU/ml for Adeno-X: TRE-ΔFosB-EGFP (ΔFosB-EGFP), $\sim 7.79 \times 10^8$ PFU/ml for Adeno-X:TRE-EGFP (EGFP alone) and $\sim 1.85 \times 10^9$ PFU/ml for Adeno-X Tet-Off virus. Cultured cells were infected with various recombinant adenoviruses at an MOI of 1 PFU/cell. Cells were coinfected with Adeno-X Tet-Off virus to supply tTA, a tetracycline-controlled transactivator.

Real-time RT-PCR analysis

The primers used to amplify the 5' common region for *fosB* and *ΔfosB* mRNA (FB1775F: GAGGAAAAGGCAGAGCTGGA; FB1855R: TGGGCC ACCAGGACAAACT), the 3' region specific for *fosB* (FBO1925F: CCAGGGTCAACATCCGCT; FBO2016R: CGTCTCGGCTGCTCTGGA) and primers used to amplify the *c-Jun* mRNA (CJN807F: CTCCAAGTG CCGGAAAAGG; CJN961R: TGTTAACGTGGTTCATGACTTTCTG) were obtained from FASMAC Co., Ltd. (Kanagawa, Japan). Specific TaqMan probes labeled with FAM (5') and TAMURA (3') for real-time PCR detection (FB1797T: CGGAGATCGCCGAGCTGCAAAA; FBO1965T: TGCTGCCGCCCCCTCCA; and CJN905T: ACATGCTCAGGGAACAGG TGGCACAG were obtained from Applied Biosystems (Foster City, CA, USA). TaqMan gene expression assays for *JunB* (Rn0059045), *JunD* (Rn00824678), *Cdk5* (Rn00590045), *GluR2* (Rn00568514), *Mmp3* (Rn00591740), *Gfap* (Rn00566603) and *Nestin* (Rn00564394) were purchased from Applied Biosystems. Total RNA was prepared from cortical cells using RNeasy Mini kit (Qiagen KK, Tokyo, Japan), and purified RNA was treated with RNase-free DNase, according to the manufacturer's instructions. cDNAs were synthesized by first-strand cDNA synthesis kit using random hexamer as the primer (Amersham Biosciences KK, Tokyo, Japan). RT-PCR and the detection of the PCR product in real time were performed using ABI PRISM 7000 Sequence Detection System (Applied Biosystems). Serially diluted cDNA was used to obtain a standard curve for each transcript.

Evaluation of cell viability

Rat embryonic cortical cells were plated in 96-well PEI-coated plates at a density of $2.67 \times 10^5/cm^2$ with 10 μM AraC (Wako Pure Chemical Industries, Osaka, Japan), or $1.67 \times 10^5/cm^2$ without AraC. After withdrawal of B27 supplement from the cultures, the cell viability was measured by monosodium salt WST-8 using the Cell Counting Kit-8 (Wako). Absorbance of WST-8 formazan dye at 450 nm was measured and the relative cell viability was determined by comparing the ratio of absorbance for each experiment with that for the control experiments. In order to evaluate the viabilities of cells infected with various recombinant adenoviruses, numbers of EGFP-positive cells in 96-well plates were counted on images captured by a digital camera. The same areas were repeatedly monitored for a week, and relative cell viability was determined by comparing the ratio of cell number for each experiment to that for the control experiments.

Decline of FosB and ΔFosB expression by Tet-off system

Rat embryonic cortical cells were cultured for 3 days in a Neurobasal medium with B27 supplement and then infected with each recombinant adenovirus together with Adeno-X Tet-Off vector. At 2 days after infection, the culture medium was changed to a Neurobasal medium lacking B27 supplement. At 13 days after infection, the culture medium was changed to a Neurobasal medium with B27 supplement and doxycycline (final 400 ng/ml; Wako). At 17 days after infection, the cells were fixed and subjected to immunofluorescence microscopy.

Injection of adenovirus vector

Rats were anesthetized with amobarbital (100 mg/kg i.p.), and a small burr hole was made in the parietal region (1.0 mm anterior and 1.6 mm right lateral from the bregma) with a dental drill. A 27-G needle on a Hamilton syringe was stereotaxically inserted into the right LV (3.8 mm in depth), and 6 μl of viral suspension ($\sim 2.34 \times 10^6$ PFU of each recombinant adenovirus expressing FosB-EGFP, ΔFosB-EGFP or EGFP alone, together with $\sim 5.55 \times 10^6$ PFU of Adeno-X Tet-Off virus) was injected

for over 6 min. At 54 h after injection, the rats were anesthetized and perfused transcardially, and the brains were processed as described in the Immunohistochemistry section. After cryoprotection with 25% sucrose in 0.1 M PBS, coronal sections (20 μm) were prepared and subjected to immunofluorescence microscopy.

Laser-scanning fluorescence microscopy

Confocal images were acquired under Eclipse TE300 (Nikon, Kanagawa, Japan) equipped with the Radiance 2100 laser-scanning fluorescence microscope system (Bio-Rad Laboratories, Hercules, CA, USA).

Image processing

All digitized images were processed for publication using the Adobe Photoshop 5.5J software package (Adobe Systems).

Statistical analysis

The data are expressed as the mean $\pm$ S.D. All data were compared using the Mann–Whitney *U*-test. Statistical significance was accepted at a level of $P<0.05$.

Acknowledgements

We thank Drs. Kunihiko Sakumi, Daisuke Tsuchimoto and Masato Furuichi for their helpful discussions, Setsuko Kitamura and Keiko Aiura for their technical assistance and Dr. B Quinn for comments on the manuscript. This work was supported by grants from CREST, Japan Science and Technology Agency, the Ministry of Education, Culture, Sports, Science, and Technology of Japan (Grant 16012248) and the Japan Society for the Promotion of Science (Grants: 15590347 and 16390119).

References

1. Nakabeppu Y, Ryder K and Nathans D (1988) DNA binding activities of three murine Jun proteins: stimulation by Fos. Cell 55: 907–915
2. Chinenov Y and Kerppola TK (2001) Close encounters of many kinds: Fos–Jun interactions that mediate transcription regulatory specificity. Oncogene 20: 2438–2452
3. Jochum W, Passegué E and Wagner EF (2001) AP-1 in mouse development and tumorigenesis. Oncogene 20: 2401–2412
4. Shaulian E and Karin M (2001) AP-1 in cell proliferation and survival. Oncogene 20: 2390–2400
5. Nakabeppu Y and Nathans D (1991) A naturally occurring truncated form of FosB that inhibits Fos/Jun transcriptional activity. Cell 64: 751–759
6. Chen J, Kelz MB, Hope BT, Nakabeppu Y and Nestler EJ (1997) Chronic Fos-related antigens: stable variants of ΔFosB induced in brain by chronic treatments. J. Neurosci. 17: 4933–4941
7. Sabatakos G, Sims NA, Chen J, Aoki K, Kelz MB, Amling M, Bouali Y, Mukhopadhyay K, Ford K, Nestler EJ and Baron R (2000) Overexpression of ΔFosB transcription factor(s) increases bone formation and inhibits adipogenesis. Nat. Med. 6: 985–990
8. Metz R, Kouzarides T and Bravo R (1994) A C-terminal domain in FosB, absent in FosB/SF and Fra-1, which is able to interact with the TATA binding protein, is required for altered cell growth. EMBO J. 13: 3832–3842
9. Dobrazanski P, Noguchi T, Kovary K, Rizzo CA, Lazo PS and Bravo R (1991) Both products of the *fosB* gene, FosB and its short form, FosB/SF, are transcriptional activators in fibroblasts. Mol. Cell. Biol. 11: 5470–5478
10. Chen J, Zhang Y, Kelz MB, Steffen C, Ang ES, Zeng L and Nestler EJ (2000) Induction of cyclin-dependent kinase 5 in the hippocampus by chronic electroconvulsive seizures: role of ΔFosB. J. Neurosci. 20: 8965–8971
11. McClung CA and Nestler EJ (2003) Regulation of gene expression and cocaine reward by CREB and ΔFosB. Nat. Neurosci. 6: 1208–1215
12. Herdegen T and Leah JD (1998) Inducible and constitutive transcription factors in the mammalian nervous system: control of gene expression by Jun, Fos and Krox, and CREB/ATF proteins. Brain Res. Brain Res. Rev. 28: 370–490
13. McGahan L, Hakim AM, Nakabeppu Y and Robertson GS (1998) Ischemia-induced CA1 neuronal death is preceded by elevated FosB and Jun expression and reduced NGFI-A and JunB levels. Mol. Brain Res. 56: 146–161
14. Liu J, Solway K, Messing RO and Sharp FR (1998) Increased neurogenesis in the dentate gyrus after transient global ischemia in gerbils. J. Neurosci. 18: 7768–7778
15. Gage FH (2000) Mammalian neural stem cells. Science 287: 1433–1438
16. Jin K, Minami M, Lan JQ, Mao XO, Batteur S, Simon RP and Greenberg DA (2001) Neurogenesis in dentate subgranular zone and rostral subventricular zone after focal cerebral ischemia in the rat. Proc. Natl. Acad. Sci. USA 98: 4710–4715
17. Nakatomi H, Kuriu T, Okabe S, Yamamoto S, Hatano O, Kawahara N, Tamura A, Kirino T and Nakafuku M (2002) Regeneration of hippocampal pyramidal neurons after ischemic brain injury by recruitment of endogenous neural progenitors. Cell 110: 429–441
18. Nakabeppu Y, Oda S and Sekiguchi M (1993) Proliferative activation of quiescent Rat-1A cells by ΔFosB. Mol. Cell. Biol. 13: 4157–4166
19. Oda S, Nishida J, Nakabeppu Y and Sekiguchi M (1995) Stabilization of cyclin E and cdk2 mRNAs at G1/S transition in Rat-1A cells emerging from the G0 state. Oncogene 10: 1343–1351
20. Nishioka T, Sakumi K, Miura T, Tahara K, Horie H, Kadoya T and Nakabeppu Y (2002) *fosB gene products trigger cell proliferation and morphological alteration* with an increased expression of a novel processed form of galectin-1 in the rat 3Y1 embryo cell line. J. Biochem. 131: 653–661
21. Tahara K, Tsuchimoto D, Tominaga Y, Asoh S, Ohta S, Kitagawa M, Horie H, Kadoya T and Nakabeppu Y (2003) ΔFosB, but not FosB, induces delayed apoptosis independent of cell proliferation in the Rat1a embryo cell Line. Cell Death Differ. 10: 496–507
22. Miura T, Takahashi M, Horie H, Kurushima H, Tsuchimoto D, Sakumi K and Nakabeppu Y (2004) Galectin-1β, a natural monomeric form of galectin-1 lacking its six amino-terminal residues promotes axonal regeneration but not cell death. Cell Death Differ. 11: 1076–1083
23. Yao H, Sadoshima S, Ooboshi H, Sato Y, Uchimura H and Fujishima M (1991) Age-related vulnerability to cerebral ischemia in spontaneously hypertensive rats. Stroke 22: 1414–1418
24. Hotta Y, Honda T, Naito M and Kuwano R (2003) Developmental distribution of coxsackie virus and adenovirus receptor localized in the nervous system. Brain Res. Dev. Brain Res. 143: 1–13
25. Sato Y, Shiraishi Y and Furuichi T (2004) Cell specificity and efficiency of the Semliki forest virus vector- and adenovirus vector-mediated gene expression in mouse cerebellum. J. Neurosci. Methods 137: 111–121
26. Brewer GJ (1995) Serum-free B27/Neurobasal medium supports differentiated growth of neurons from the striatum, substantia nigra, septum, cerebral cortex, cerebellum, and dentate gyrus. J. Neurosci. Res. 42: 674–683
27. Cheng A, Wang S, Yang D, Xiao R and Mattson MP (2003) Calmodulin mediates brain-derived neurotrophic factor cell survival signaling upstream of Akt kinase in embryonic neocortical neurons. J. Biol. Chem. 278: 7591–7599
28. Herdegen T, Claret FX, Kallunki T, Martin-Villalba A, Winter C, Hunter T and Karin M (1998) Lasting N-terminal phosphorylation of c-Jun and activation of c-Jun N-terminal kinases after neuronal injury. J. Neurosci. 18: 5124–5135
29. Herdegen T and Waetzig V (2001) AP-1 proteins in the adult brain: facts and fiction about effectors of neuroprotection and neurodegeneration. Oncogene 20: 2424–2437
30. Doetsch F, García-Verdugo JM and Alvarez-Buylla A (1997) Cellular composition and three-dimensional organization of the subventricular germinal zone in the adult mammalian brain. J. Neurosci. 17: 5046–5061
31. Fukuda S, Kato F, Tozuka Y, Yamaguchi M, Miyamoto Y and Hisatsune T (2003) Two distinct subpopulations of nestin-positive cells in adult mouse dentate gyrus. J. Neurosci. 23: 9357–9366
32. Garcia AD, Doan NB, Imura T, Bush TG and Sofroniew MV (2004) GFAP-expressing progenitors are the principal source of constitutive neurogenesis in adult mouse forebrain. Nat. Neurosci. 7: 1233–1241
33. Nakabeppu Y and Nathans D (1989) The basic region of Fos mediates specific DNA binding. EMBO J. 8: 3833–3841

34. Murphy TH, Worley PF, Nakabeppu Y, Christy B, Gastel J and Baraban JM (1991) Synaptic regulation of immediate early gene expression in primary cultures of cortical neurons. J. Neurochem. 57: 1862–1872
35. Horie H, Inagaki Y, Sohma Y, Nozawa R, Okawa K, Hasegawa M, Muramatsu N, Kawano H, Horie M, Koyama H, Sakai I, Takeshita K, Kowada Y, Takano M and Kadoya T (1999) Galectin-1 regulates initial axonal growth in peripheral nerves after axotomy. J. Neurosci. 19: 9964–9974
36. Smith ML, Bendek G, Dahlgren N, Rosén I, Wieloch T and Siesjö BK (1984) Models for studying long-term recovery following forebrain ischemia in the rat. 2. A 2-vessel occlusion model. Acta Neurol. Scand. 69: 385–401

Cell Death and Differentiation (2004) 11, 1076–1083

www.nature.com/cdd

Galectin-1β, a natural monomeric form of galectin-1 lacking its six amino-terminal residues promotes axonal regeneration but not cell death

T Miura[1,2], M Takahashi[3], H Horie[4], H Kurushima[1,2], D Tsuchimoto[1,2], K Sakumi*[,1,2] and Y Nakabeppu[1,2]

[1] Division of Neurofunctional Genomics, Department of Immunobiology and Neuroscience, Medical Institute of Bioregulation, Kyushu University, Maidashi Higashi-ku, Fukuoka, Japan
[2] Core Research for Evolutional Science and Technology (CREST), Japan Science and Technology Agency (JST), Japan
[3] Research Group FRE 2230, CNRS and Université de Nantes, Nantes, France
[4] Advanced Research Center for Biological Science, Waseda University, 2-7-5 Higashifushimi, Nishitokyo City, Tokyo, Japan
* Corresponding author: K Sakumi, 3-1-1 Maidashi, Higashi-ku, Fukuoka 812-8582, Japan. Tel: +81 92 642 6800; Fax: +81 92 642 6791; E-mail: sakumi@bioreg.kyushu-u.ac.jp

Received 02.3.04; revised 05.4.04; accepted 05.4.04; published online 04.6.04
Edited by H Ichijo

Abstract

We previously identified a novel N-terminally processed form of galectin-1, galectin-1β (Gal-1β) whose expression was induced by ΔFosB. In the present study, the biochemical properties and biological functions of Gal-1β were compared with the full-length form of galectin-1 (Gal-1α). We first purified recombinant mouse Gal-1α and β (rmGal-1α, β) to near homogeneity. The rmGal-1α exists as a monomer under oxidized conditions and forms a dimer under reduced conditions, while the rmGal-1β exists as a monomer regardless of redox conditions. The affinity of rmGal-1β to β-lactose was approximately two-fold lower than that of rmGal-1α under reduced conditions. The viability of Jurkat cells efficiently decreased when they were exposed to rmGal-1α, however, rmGal-1β barely induced such a reduction. In contrast, both rmGal-1α and rmGal-1β exhibited an equivalent capacity to promote axonal regeneration from the dorsal root ganglion explants. Our results suggest that the biochemical properties of rmGal-1β determine its biological functions.

Cell Death and Differentiation (2004) **11**, 1076–1083.
doi:10.1038/sj.cdd.4401462
Published online 4 June 2004

Keywords: galectin-1; ΔFosB; redox; cell viability; axonal regeneration

Abbreviations: Gal-1, Galectin-1; AP-1, activator protein-1; β-ME, β-mercaptoethanol; CD, circular dichroism; DRG, dorsal root ganglion

Introduction

In mammals, the regulation of the cell fate to either proliferate, differentiate, arrest cell growth, or initiate programmed cell death is the most fundamental mechanism to maintain normal cell function and tissue homeostasis. Under multiple signaling pathways, Jun and Fos family proteins play important roles as components of an AP-1 (activator protein-1) complex,[1,2] to regulate the transcription of various genes involved in cell proliferation, differentiation, and programmed cell death.[3,4] We previously reported that ΔFosB, one of AP-1 subunits encoded by alternatively spliced *fosB* mRNA,[5] triggers one round of proliferation in the quiescent rat embryo cell lines, rat3Y1 and rat1a, followed by a different cell fate such as morphological alteration or delayed cell death, respectively.[6,7] As one of the downstream targets of ΔFosB in rat3Y1 cell line, we identified a novel form of rat galectin-1 whose N-terminal residue corresponds to the seventh residue of the already-known form of galectin-1 (Gal-1α). We named this novel processed form of galectin-1 as galectin-1β (Gal-1β).[6] We have previously shown that the expression of galectin-1 is required for the proliferative activation of quiescent rat1a cells by ΔFosB, indicating that galectin-1 is one of the functional targets of ΔFosB to modulate cell fate.[7]

Galectin family protein is defined by its affinity for β-galactoside sugars and shared amino-acid sequence which encodes the carbohydrate-binding-domain (CRD),[8] and 10 mouse proteins are now registered in the database. Galectin-1, one of the well-studied proteins among the known galectin families is a 14.5-kDa protein with a single CRD in the molecule. Galectin-1 is expressed in many tissues including skeletal muscle, liver, spleen, and lung.[9–14] It has been documented that galectin-1 is a multifunctional molecule involved in the regulation of either cell–cell[15] or cell–extracellular matrix adhesion,[16] cell proliferation,[7,17] programmed cell death,[18,19] the Ras signaling pathway,[20,21] and is also related to the mRNA splicing mechanism.[22,23]

The amino-terminal alanine residue of Gal-1α is acetylated after the removal of the first methionine residue (Figure 1a)[24] and Gal-1α forms a homodimer in physiological conditions (Figure 1b).[25,26] Recently, it has been shown that a monomeric form of oxidized Gal-1α strongly promotes axonal regeneration after axotomy in the peripheral nerves.[27–29] Because Gal-1β lacks the N-terminal six residues, which were reported to be important for the dimer formation of Gal-1α[26,30] (Figure 1a), it is most likely that Gal-1α and Gal-1β exhibit distinct biological functions with different biochemical properties.

To explore the distinct biochemical properties of Gal-1β, the recombinant proteins of mouse Gal-1α and Gal-1β were expressed in *Escherichia coli* cells and then were purified to near homogeneity. In the present study, we report that the affinity of Gal-1β to lactose is 2.27-fold lower than that of Gal-1α and Gal-1β is present in a monomeric form regardless of the redox conditions, and that Gal-1β promotes axonal regeneration as does Gal-1α, however, it has much less cytotoxicity.

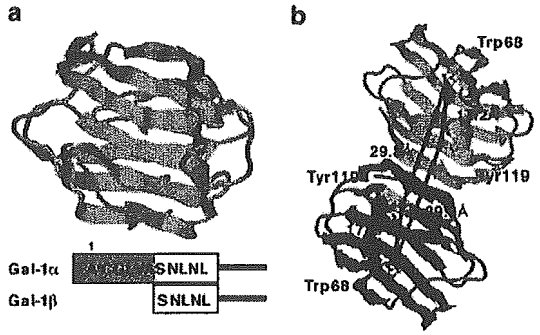

Figure 1 Crystal structure of galectin-1. (**a**) The structure of a bovine heart galectin-1 (Gal-1α). Six amino-acid residues which are missing in Gal-1β are shown in dark gray and the acetylated alanine at the N-terminus of Gal-1α is refered as the first residue in the present study. The amino-acid sequences of N-terminal parts of Gal-1α and Gal-1β are also shown. (**b**) The structure of Gal-1α homodimer. The crystal structure of bovine Gal-1α dimer (PDB 1SLA) are shown by Protein Explorer.[50] The Trp68 and Tyr119 residues are shown with the side chains. The distance between Trp68 and Tyr119 of the same molecule and that of another molecule formed homodimer are shown

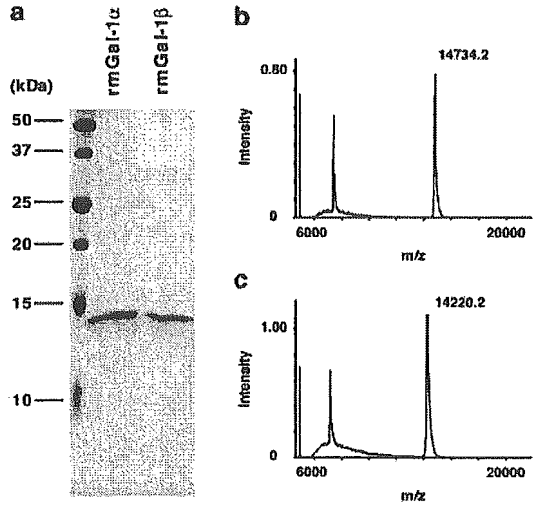

Figure 2 Purified preparations of rmGal-1α and rmGal-1β. (**a**) 1 μg of purified rmGal-1α and rmGal-1β were separated on a 15% SDS-PAGE gel. (**b, c**) MALDI-TOF mass spectrometric analyses of rmGal-1α (**b**) and rmGal-1β (**c**)

Results

Expression and purification of rmGal-1α and rmGal-1β

Amino-acid sequences of galectin-1 are well conserved among mammals, and more than 90% of them are identical among rat, mouse, and human. In the present study, we prepared and characterized recombinant mouse Gal-1α and Gal-1β (rmGal-1α, β).

Both rmGal-1α and rmGal-1β expressed in *E. coli* cells were soluble in the presence of 14 mM β-ME, and thus were purified by affinity chromatography with lactose-agarose. During affinity chromatography, we found that a substantial amount of rmGal-1β, but not rmGal-1α, was recovered in the flow-through fractions (data not shown). The rmGal-1β that was recovered in the flow-through fractions is not an inactivated form because when it was reapplied onto the same column, essentially the same elution pattern was obtained.

An SDS-PAGE analysis revealed that each preparation of rmGal-1α and rmGal-1β was almost nearly homogenous (Figure 2a), and their molecular mass determined by the MALDI-TOF analysis was 14734.2 and 14220.2 Da, respectively (Figure 2b, c). The values correspond to the molecular mass of each protein lacking the N-terminal methionine residue.

The secondary structures of rmGal-1β

rmGal-1β lacks six residues present in the N-terminus of rmGal-1α. To examine whether this difference affected in the secondary structures between rmGal-1α and rmGal-1β, the CD spectrum of each protein was measured (Figure 3a). The CD spectra of both proteins exhibited a major negative peak around 215 nm, and this peak of rmGal-1β was about 15% weaker in intensity than that of rmGal-1α, suggesting that each protein has similar secondary structures of which major components are β-sheet structure,[31,32] and that rmGal-1β lacks the N-terminal β-sheet.

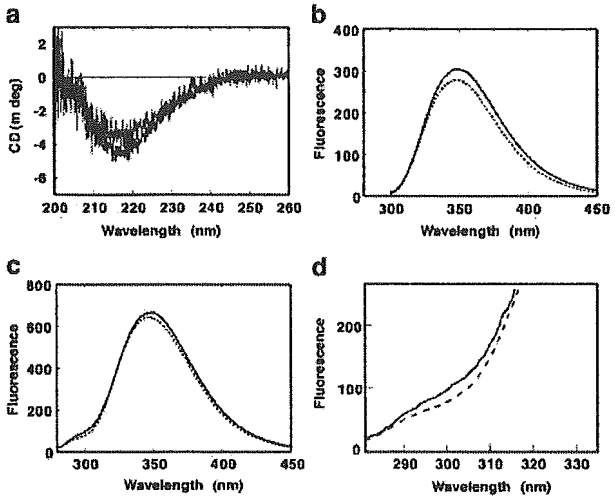

Figure 3 CD spectra and intrinsic fluorescence emission spectra of rmGal-1α and rmGal-1β. (**a**) CD spectra of rmGal-1α and rmGal-1β. CD spectra of 0.01 mg/ml rmGal-1α (black line) and rmGal-1β (gray line) were measured. (**b, c**) The fluorescence emission spectra of rmGal-1α and rmGal-1β. The emission spectra of rmGal-1α (dashed line) and rmGal-1β (solid line) were measured under the same conditions as in CD measurement with excitation at 295 nm (**b**) or at 270 nm (**c**). (**d**) The difference between the fluorescence emission spectra of rmGal-1α and that of rmGal-1β with excitation at 270 nm. The short-range emission spectra (280–330 nm) of rmGal-1α (dashed line) and rmGal-1β (solid line) are shown

We next examined the protein fluorescence of rmGal-1α and rmGal-1β. Gal-1α has a single residue of tryptophan (Trp68) and tyrosine (Tyr119), which are conserved at the corresponding positions of Gal-1β.[25,33] Upon selective excitation of tryptophan residue at 295 nm, emission spectrum of rmGal-1α peaked at 348 nm (Figure 3b), and that of rmGal-1β peaked at 351 nm (Figure 3b).

We also measured protein fluorescence with excitation at 270 nm, which came from both tryptophan and tyrosine

residues. The emission spectra of rmGal-1α and rmGal-1β with excitation at 270 nm exhibited a small additional peak around 300 nm (Figure 3c, d) that from tyrosine residue,[34] and this peak was larger from rmGal-1β than rmGal-1α. In addition, the intensity of tryptophanyl fluorescence around 350 nm for rmGal-1β was almost the same as that for rmGal-1α, while it was larger when excited at 295 nm. The ratio of intensity of tryptophanyl fluorescence at 360 nm with excitation at 270 and 295 nm (I_{ex270}/I_{ex295}) was higher for rmGal-1α than for rmGal-1β. This fact revealed that the fluorescence energy transfer from Tyr119 to Trp68 residues occurs more efficiently in rmGal-1α than in rmGal-1β. Indeed, the estimated distance between Trp68 residue in one subunit and Tyr119 in another subunit of a Gal-1α dimer is 29.3 Å, and is close enough for efficient energy transfer (Figure 1b).[34]

rmGal-1β exists as a monomer while rmGal-1α forms a homodimer under reduced conditions

Gal-1α has been reported to form a homodimer in a concentration-dependent manner,[35] and that hydrophobic amino-acid residues at both N- and C-terminal parts are important in its dimerization.[26,30]

We performed a size-exclusion HPLC analysis to separate the dimer and monomer forms of rmGal-1α and rmGal-1β (Figure 4). To avoid their spontaneous oxidation during the experiments, each protein was prepared in PBS containing 4 mM β-ME and the same buffer was used as the solvent for HPLC. Under our conditions, the retention time of each preparation was 9.5 min for rmGal-1α and 10.5 min for rmGal-1β (Figure 4a), respectively, indicating that rmGal-1α behaves as a dimer while rmGal-1β as a monomer. We found that

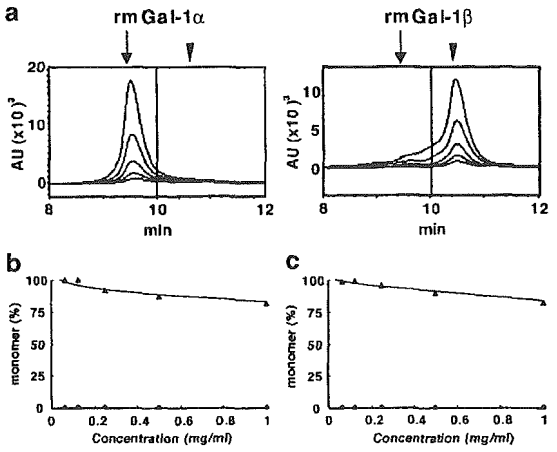

Figure 4 Dimerization of rmGal-1α and rmGal-1β did not depend on its concentration under reduced condition. (**a**) Monomer–dimer equilibrium of rmGal-1α and rmGal-1β. rmGal-1α or rmGal-1β was serially diluted from 1 to 0.0625 mg/ml with PBS containing 4 mM β-ME, and were incubated at 4°C at least for 20 h, and then 10 μl of each sample was applied to the size-exclusion HPLC. A chromatogram of each analysis was overlaid. The arrowhead indicates an elution peak of a monomer form and the arrow indicates that of a dimer form. (**b**) Content of monomer formed at different concentrations of each rmGal-1α (circles) and rmGal-1β (triangles) was estimated from the peak areas, and plotted against concentration of each protein. (**c**) The content of the monomer formed at different concentrations of each rmGal-1α (circles) and rmGal-1β (triangles) in the presence of 10 mM β-lactose was estimated and plotted

rmGal-1α behaved exclusively as a dimer at concentrations from 0.0625 mg/ml (4.2 μM) to 1.0 mg/ml (67 μM). In contrast, rmGal-1β behaved mostly as a monomer with a slight trend to form a dimer at higher concentrations (Figure 4a, b). Essentially, the same results were obtained when experiments were performed with a buffer containing 10 mM β-lactose (Figure 4c).

Monomerization of rmGal-1α depends on oxidation

Our results indicate that rmGal-1α forms a dimer under reduced conditions. On the other hand, Inagaki *et al*.[29] showed that human Gal-1α oxidized *in vitro* by air is a monomeric form. Therefore, we examined the possibility that the monomer–dimer equilibrium of rmGal-1α may be modulated by redox conditions. Alterations of the monomer–dimer equilibrium of rmGal-1α during spontaneous oxidation by air at 4°C in the presence of various concentrations of β-ME, were monitored by size-exclusion HPLC for 50 days (Figure 5a). The content of the monomer form of rmGal-1α increased in a time-dependent manner in the absence or presence of a lower concentration of β-ME (0.7 mM), and in the former conditions more monomers were formed (Figure 5a). In the presence of 14 mM β-ME, rmGal-1α remained as a dimer for at least 50 days. Spontaneously oxidized rmGal-1α by incubation in the absence of β-ME for 50 days, in which 80% was a monomer, was completely converted to a dimer 24 h after incubation in the presence of 14 mM β-ME (Figure 5b, d). A monomeric form of rmGal-1α that oxidized in the presence of Cu^{2+} was partially converted to a dimeric form 24 h after incubation in the presence of 4 mM β-ME (Figure 5c, e). In contrast, rmGal-1β was a monomer form, regardless of incubation for 3 days in the presence of β-ME (Figure 5a).

We thus concluded that the monomer–dimer equilibrium of rmGal-1α is determined by the redox condition.

Lectin activity of rmGal-1α and rmGal-1β

The sugar binding activity is another function of galectin-1. To compare their affinity to β-lactose quantitatively, we used fluorescence spectroscopy to examine the concentration-dependent quenching of the tryptophanyl fluorescence by β-lactose, since Trp68 residue resides in the lactose binding domain of galectin-1.[25] The addition of β-lactose decreased the fluorescence intensity of both rmGal-1α and rmGal-1β in a concentration-dependent manner (Figure 6), and the fluorescence peak was shifted to shorter wavelength (data not shown). The binding constant of each protein for β-lactose was calculated with a simple binding model of one β-lactose molecule per subunit without any cooperativity (K_d = 0.22 mM for rmGal-1α and 0.50 mM for rmGal-1β) (Figure 6).

Next, we examined the hemagglutination activity of rmGal-1α and rmGal-1β. In the absence of β-lactose, rmGal-1α and rmGal-1β induced agglutination at concentrations of ⩾0.98 and ⩾15.6 μg/ml, respectively (Figure 6b). The hemagglutination of each protein was inhibited in the presence of 5 mM β-lactose, thus confirming that this hemagglutination was a specific activity of each protein (Figure 6b).

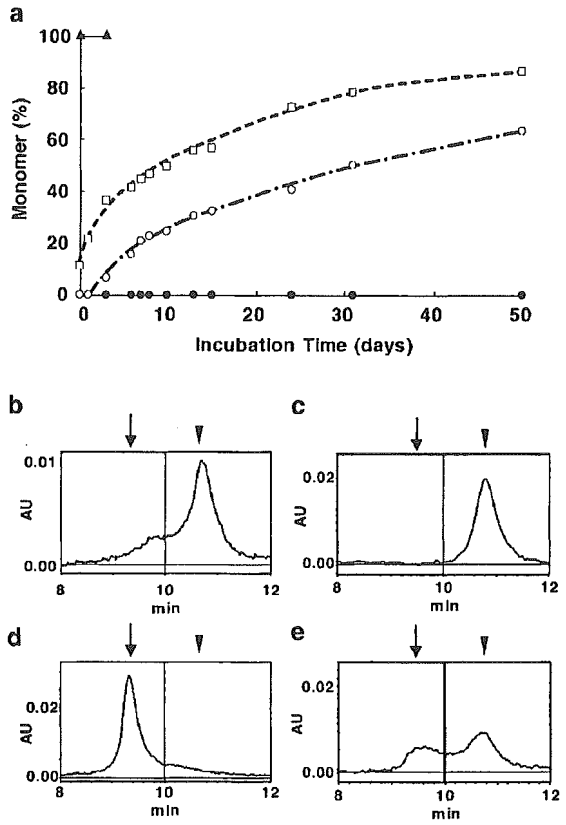

Figure 5 Dimerization of rmGal-1α depends on redox conditions. (**a**) Spontaneous oxidation of rmGal-1α. rmGal-1α were prepared at the concentrations of 0.1 mg/ml in PBS with 14 mM β-ME (closed circles) or 0.7 mM β-ME (open circles) or no β-ME (open squares). After incubation at 4°C for the indicated periods, the content of monomeric rmGal-1α was determined by the size-exclusion HPLC. The content of monomeric rmGal-1β incubated in the presence of 14 mM β-ME for 3 days was also determined (closed triangles). (**b**) Oxidized rmGal-1α by air exists mostly as a monomer. rmGal-1α, oxidized at 4°C for 50 days in the absence of reducing agent was applied to the size-exclusion HPLC. (**c**) Oxidized rmGal-1α exists as a monomer. The oxidized rmGal-1α in the presence of $CuSO_4$ as described in the Materials and Methods, was analyzed by the size-exclusion HPLC. (**d**) Reversible dimer formation of spontaneously oxidized rmGal-1α. The oxidized rmGal-1α shown in (**b**) was incubated in the presence of 14 mM β-ME for 24 h at 4°C, and then was analyzed by size-exclusion HPLC. (**e**) Reversible dimer formation of oxidized rmGal-1α. The oxidized rmGal-1α shown in (**d**) was incubated in the presence of 4 mM β-ME at 4°C for 24 h, and then it was applied to the size-exclusion HPLC. The arrowhead indicates the elution peak of a monomer form and the arrow indicates that of a dimer form

rmGal-1β lacks an ability to decrease the cell viability

It has been established that Gal-1α has an ability to induce apoptosis in activated T cells or some leukemic cell lines such as Jurkat cells.[18,36–38] We thus examined whether the viability of Jurkat cells decreases with rmGal-1β in comparison to rmGal-1α. With 0.1 mg/ml or higher concentrations of rmGal-1α the viability of Jurkat cells effectively decreased in comparison with PBS control (Figure 7a). In contrast, much higher concentrations of rmGal-1β slightly decreased the viability of Jurkat cells. After exposure to 0.2 mg/ml of rmGal-1α, the viability of Jurkat cells decreased to 75% the

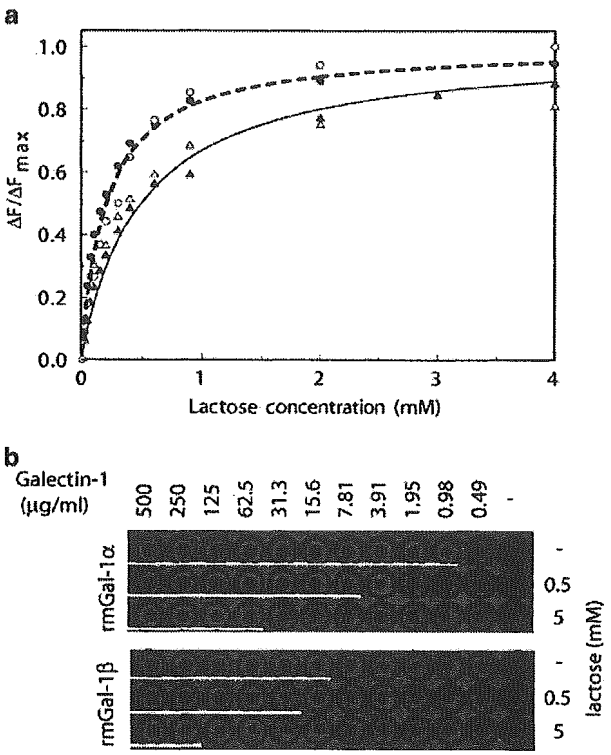

Figure 6 Lectin activity of rmGal-1α and rmGal-1β. (**a**) Lactose binding activity of rmGal-1α or rmGal-1β. Lactose binding activity of rmGal-1α (circles) or rmGal-1β (triangles) was monitored by their fluorescence change with step-wise addition of β-lactose. The concentrations of each protein were 50 nM (open symbols) and 500 nM (closed symbols). The best-fit curves for rmGal-1α ($K_d = 0.22$ mM) and rmGal-1β ($K_d = 0.50$ mM) are shown. (**b**) Hemagglutination activities (HA) of rmGal-1α and rmGal-1β. The hemagglutination activities of rmGal-1α and rmGal-1β were determined as previously described.[29] In brief, 50 μl of 2% (v/v) suspension of glutaraldehyde stabilized rabbit red blood cell (INTER-CELL TECHNOLOGIES) was mixed with 50 μl of various concentrations of rmGal-1α or rmGal-1β (0.98 μg/ml to 1 mg/ml) prepared in PBS containing 4 mM β-ME. After incubation at room temperature for 1 h, the hemagglutinating activity was determined based on the sedimentary state of the erythrocytes. The hemagglutinating activity was also determined in the presence of 5 mM or 0.5 mM of β-lactose. All reactions were performed with U-bottom 96-well microtiter plates (Falcon). The white bars indicate HA(+) wells

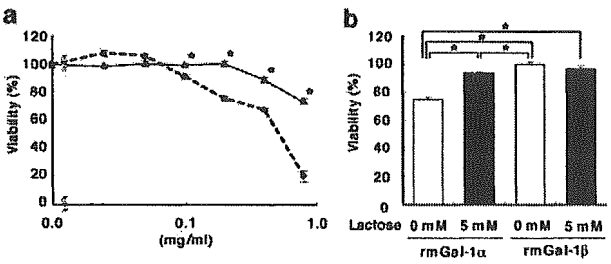

Figure 7 Effects of rmGal-1α and rmGal-1β on the viability of Jurkat cells. (**a**) The viabilities of Jurkat cells after exposure to rmGal-1α or rmGal-1β. Jurkat cells were exposed to indicated concentrations of rmGal-1α (circles) and rmGal-1β (triangles) for 24 h. The data are expressed as the mean ± S.E.M. ($n = 4$–12), and then were statistically compared using Mann–Whitney *U*-tests (*$P < 0.05$). (**b**) Effects of β-lactose on the function of rmGal-1α or rmGal-1β. The viabilities of Jurkat cells after exposure to a concentration of 0.2 mg/ml of rmGal-1α or rmGal-1β with (closed bars) or without β-lactose (open bars). The data are expressed as the mean ± S.E.M. ($n = 8$–12), and then are statistically compared by ANOVA (Games–Howell test for multiple comparisons, *$P < 0.05$)

level of the control, while in the presence of 5 mM β-lactose, it was restored to 94% of the control. On the other hand, rmGal-1β did not decrease the viability of Jurkat cells at all with or without β-lactose (Figure 7b).

rmGal-1β promotes axonal regeneration as efficient as does rmGal-1α

Horie *et al*.[28,29] reported that oxidized human galectin-1 has no lectin activity and behaves as a monomer but it efficiently promotes the regeneration of axons from rat DRG explants. We next examined whether rmGal-1β as well as rmGal-1α has activity to promote axonal regeneration (Figure 8). To eliminate any deleterious effects of β-ME, we prepared each protein in PBS lacking β-ME. The number of regenerating axons from the central site of the DRG explants increased significantly with both rmGal-1α and rmGal-1β in a dose-dependent manner (Figure 8c). With 0.5 or 5 ng/ml of each protein, about 1.5 times more axons were regenerated from the central site of the DRG explants in comparison to those in the control. In contrast, from the peripheral site of the explants, the maximal number of regenerating axons was observed at a concentration of 0.5 ng/ml of each protein, and about 1.5 times more axons were regenerated in comparison to those in the control (Figure 8d).

Discussion

In the present study, we demonstrated that rmGal-1α forms a homodimer in the presence of reducing agents, within the range of its concentration from 4.2 to 67 μM (Figure 4), and that the monomer–dimer equilibrium of rmGal-1α can be regulated by redox conditions (Figure 5). Cho and Cummings[35] reported that a mutant form (C2SrGal-1α) of recombinant Gal-1α in which the cysteine residue at position 2 (Cys2) was substituted with a serine residue, exists in a reversible monomer–dimer equilibrium with a $K_d = 7\,\mu M$. However, Giudicelli *et al*.[39] also reported that Gal-1α exists as a dimeric form even at a low concentration (2 μM) in the presence of 1 mM β-ME using recombinant human galectin-1 (rhGal-1α). There are six cysteine residues in a Gal-1α molecule, and it has been shown that the formation of disulfide bonds abolishes its β-galactosides-binding activity. In the oxidized Gal-1α, formation of a disulfide bond between residues Cys2 and Cys130 was experimentally demonstrated.[29,40] It is most likely that a structural alteration of the dimerizing surface consisting of the N- and C-terminal regions containing Cys2 and Cys130 abolishes the dimer formation. Here, we may suggest that Gal-1α is one of mediators of the cellular redox status, thus regulating cellular functions to achieve cellular adaptations to the redox status.

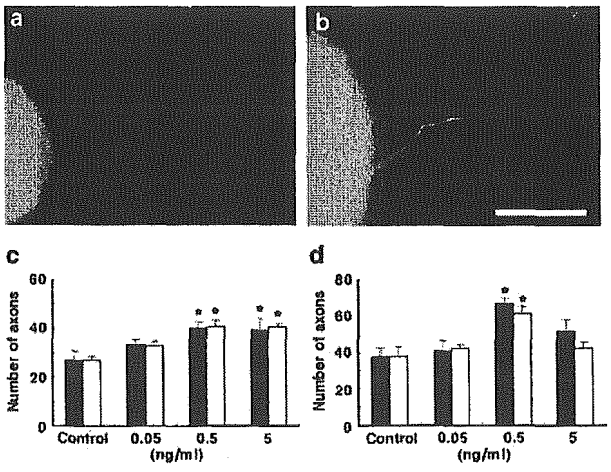

Figure 8 Effects of rmGal-1α and rmGal-1β on axonal regeneration from the DRG explants. (**a**, **b**) Immunofluorescence microscopic identification of regenerating axons from the peripheral site of adult rat DRG explants in the absence (**a**) or presence of 0.5 ng/ml of rmGal-1β (**b**) (*scale bar* = 200 μm). (**c**, **d**) Promotion of axonal regeneration by rmGal-1α and rmGal-1β. The relative number of regenerating axons from central (**c**) and peripheral (**d**) sites of the DRG explants in the presence of the indicated concentrations of rmGal-1α (closed bar) or rmGal-1β (open bar) are shown in comparison with the control. The data are expressed as the mean ± S.E.M. ($n = 8$–10), and then were statistically compared by ANOVA (Dunnett's test for multiple comparisons, $^*P < 0.05$)

We previously reported that Gal-1β, the N-terminally truncated isoform of Gal-1α was identified as one of molecules whose expression is regulated by ΔFosB in cultured rat embryo cell line.[6,7] Our data obtained by size-exclusion HPLC analyses strongly suggested that rmGla-1β exists mostly as a monomer even in reduced conditions. A protein fluorescence analysis showed that the energy transfer from Tyr119 to Trp69 was smaller in rmGal-1β than in rmGal-1α which exists as a homodimer, thus indicating that the two residues are apart from each other in the former. Together with these data, we conclude that rmGal-1β exists mostly as a monomer in solution. We showed that affinity of rmGal-1β to β-lactose was reduced to 44% levels of that of rmGal-1α in reduced conditions, and rmGal-1β retained less than 1/16 levels of hemaggutinating activity observed in rmGal-1α, indicating that rmGal-1β may not behave as a divalent lectin. We thus conclude that Gal-1β is a natural monomeric form of galectin-1.

Moreover, we showed that rmGal-1β, but not rmGal-1α lacks the ability to decrease the viability of Jurkat cells in a lactose-sensitive manner (Figure 7), while rmGal-1β promotes axonal regeneration from the DRG explants as efficient as does rmGal-1α (Figure 8). These findings are consistent with the monomeric status of rmGal-1β. We thus propose that the multifunctional properties of galectin-1 are somehow attributed not only to the redox regulation but also to the presence of two distinctive isoforms, Gal-1α and Gal-1β.

In the DRG, about 20% of the neurons strongly express galectin-1, and the expression of galectin-1 is considered to likely increase after peripheral nerve injury.[41] *In vitro* studies using DRG explants revealed that oxidized Gal-1α directly stimulates macrophages to secrete a factor that promotes axonal growth;[42] however, many important questions remain to be answered. Concerning Gal-1β, we must clarify whether or not Gal-1β also acts on macrophages, and whether the oxidation of cysteine residues in Gal-1β is required for such regeneration.

In the central nervous system, galectin-1 in the olfactory system has been shown to be involved in neurite outgrowth and synaptic connectivity during development. In contrast, the expression of ΔFosB is highly inducible in the adult brain in

response to various insults such as ischemic reperfusion injury,[43] seizure induced by electric stimulation or cocaine administration.[44,45] We have shown that the expression of ΔFosB in cultured cells modulates the cell fate such as cell proliferation, cell differentiation, and cell death accompanied with increased expression of galectin-1.[6,7] We found that galectin-1 is indeed expressed in the adult mouse hippocampus or cortex (T Miura and Y Nakabeppu, unpublished data), and that the induction of galectin-1 occurs in the rat hippocampus after ischemic reperfusion injury (H Kurushima and Y Nakabeppu, unpublished data). These observations suggest that the two isoforms of galectin-1, both of which are likely to be induced by ΔFosB in response to brain damage, either regulate the cell fate or are involved in neurite outgrowth and synaptic connectivity of regenerating neurons. Alterations of the brain function in *galectin-1*-null and *fosB*-null mice after such insults are now being examined in our laboratory.

Materials and Methods

Plasmids

Mouse Gal-1α cDNA was amplified by PCR using first-strand cDNA prepared from mouse CCE embryonic stem cell line[46] as the template with a Gal-1α-specific primer set (GAL1-5-1: GCTGGATCCATGGCCTGTGGTCTG, GAL1-3: GCTGGATCCCTTCACTCAAAGGCCACAC), and was subcloned into pT7Blue T-vector (Novagen), to obtain pT7Blue-mGla-1α. For subcloning, a neutral mutation was introduced at the one of two *Nco*I recognition site by recombinant PCR methods using two sets of primers, (M4: GTTTTCCCAGTCACGAC, MuFw: GGCGTCTCCGTGGGCATTGAAGCGAGG) and (MuRv: AATGCCCACGGAGACGCCAACACC, RV: CAGGAAACAGCTATGAC), to obtain pBluescript-rmGal-1α. For the expression of recombinant mouse Gal-1α (rmGal-1α) in *E. coli*, a *Nco*I–*Bam*HI fragment encoding mouse Gal-1α derived from pBluescript-rmGal-1α was subcloned into a *Nco*I–*Bam*HI-digested pET8c,[47] and pET8c-rmGal-1α was obtained.

We designed a 5′-primer to place the start codon just in front of the N-terminus of mouse galectin-1β, and named GAL1-5-2 (GGTGCTAGCATGAGCAACCTGAATCTCAAACCTGG). Using pT7Blue-mGal-1α as a template, PCR was performed with a primer set of GAL1-5-2, and GAL1-3, and PCR product was subcloned into pT7Blue T-vector. A *Nde*I–*Bam*HI fragment encoding mouse Gal-1β, in which the *Nde*I-cleaved end was filled in by Klenow fragment, was subcloned into *Nhe*I/*Bam*HI cleaved pET3a,[47] in which the *Nhe*I-cleaved end was filled in by Klenow fragment, to obtain pET3a-mGal-1β. All primers used in the present study were obtained from Greiner Japan and the DNA sequences of each plasmid were all confirmed with ABI Prism Big Dye terminator cycle sequencing kit and ABI PRISM 3100 Genetic Analyzer (PE Applied Biosystems).

Expression and purification of rmGal-1α and rmGal-1β

E. coli strain of BL21 (CodonPlus RIL) cells (Stratagene) were transformed with pET8c-rmGal-1α or pET3a-mGal-1β, and then were grown in an LB medium with 50 μg/ml of ampicillin, at 37°C with vigorous shaking. Protein expression was induced by the addition of 1 mM isopropyl β-D-thiogalactoside to the cultures and cell pellets of approximately 7 g wet weight were obtained from a 2-l culture. The purification of rmGal-1α and rmGal-1β was performed as previously described,[48] with some modifications. In brief, *E. coli* cell pellets were resuspended with Buffer T (50 mM Tris-HCl (pH 7.6), 100 mM NaCl, 14 mM β-mercaptoethanol (β-ME)) supplemented with protease inhibitor cocktail (Sigma). After being disrupted by sonication, the cell lysate was clarified by centrifugation at 40 000 × *g*, for 30 min at 4°C. The recovered supernatant was applied to a column packed with lactose-agarose (Seikagaku Corporation) and bound proteins were eluted with Buffer T containing 200 mM β-lactose (Sigma). Fractions containing the recombinant protein were collected, and then were dialyzed against PBS containing with 4 mM β-ME. The dialyzed fraction was applied to Detoxi-gel column (Pierce), and the elute was filtered through Millex-GX (Millipore), and was stored at −80°C until use. Column chromatography was performed with the Äkta system (Amersham Bioscience).

Mass spectrometry analysis

Matrix-assisted laser desorption ionization-time of flight (MALDI-TOF) mass spectra of purified proteins were recorded on an Autoflex mass spectrometer (Bruker Daltonics), in the 6000–22 000 Da mass range, with Protein calibration standard I (Bruker Daltonics). A saturated solution of sinapinic acid in 30% acetonitrile/0.07% trifluoroacetic acid (vol/vol) was used as matrix.

Circular dichroism (CD) and fluorescence measurements

CD spectra were measured using a step mode (bandwidth: 2 nm; interval: 0.1 nm; response time: 0.125 s) in a J-810 CD spectrometer (Jasco) equipped with a temperature controller. The spectra were averaged over four scans. Fluorescence was measured in an F-6500 spectrofluorometer (Jasco) equipped with a temperature controller. The emission spectra (bandwidth: 3 nm; response time: 0.5 s; scan rate: 100 nm/min) were measured with excitation at 295 or at 270 nm. The spectra were averaged at least at two scans, and were corrected by subtracting the buffer signal. The experiments were mainly performed in PBS buffer with 1 mM β-ME. Some CD and fluorescence measurements were performed in 20 mM sodium phosphate with 1 mM β-ME. The buffers were degassed just before use.

Size-exclusion HPLC

To separate the monomeric and dimeric forms of rmGal-1α or rmGal-1β, size-exclusion HPLC was performed as described previously,[35] except for using Class-VP HPLC System (Shimazu) equipped with TSK-GEL superSW2000 column (Tosoh). The column was equilibrated with PBS containing 4 mM or 14 mM of β-ME and 10 μl of the sample was injected into the column. Separation was carried out isocratically at 0.35 ml/min for 25 min. The elution of protein was monitored by absorbance at 214 nm.

Preparation of oxidized rmGal-1α

rmGal-1α was oxidized in the presence of $CuSO_4$ as described previously.[29] The solution of rmGal-1α (45.5 μg/ml in 20 mM Tris-HCl (pH 8.0)) was prepared in a Slide-A-Lyzer (MWCO: 3500, Pierce), and oxidation was performed by dialysis of the solution in the Slide-A-Lyzer against the buffer containing 0.0001% (w/v) $CuSO_4$ at 4°C for 2 days. The solution was further dialyzed against 10 mM Tris-HCl (pH 7.5)/10 mM NaCl for two days, and was applied to a HitrapQ column (Amersham Biosciences). Bound Gal-1α was eluted with a linear gradient of 10 mM to

1 M NaCl in 10 mM Tris-HCl (pH 7.5), and fractions containing the monomeric Gal-1α were pooled and used as oxidized Gal-1α.

Jurkat cell culture and viability assay

The Jurkat E6.1. cell line was obtained from ATCC and cultured in RPMI1640 medium (Gibco) supplemented with 4.5 g/l glucose, 10 mM HEPES, 1 mM sodium pyruvate and 10% heat-inactivated FBS. Exponentially growing Jurkat cells were prepared at 4×10^5 cells/ml in RPMI1640 medium supplemented with 1% heat-inactivated FBS. Various concentrations of rmGal-1α or rmGal-1β were prepared in PBS containing 4 mM β-ME. A volume of 75 μl of the cell suspension was mixed with 25 μl of rmGal-1α or rmGal-1β solution in flat-bottom 96-well microtiter plates (Sumilon), and the mixture was incubated at 37°C in a CO_2 incubator for 24 h. The number of viable cells was estimated by CellTiter-Glo™ Luminescent Cell Viability Assay (Promega) and Walloc 1420 ARVO *multilabel counter (Perkin-Elmer)*.

Assay for axonal regeneration *in vitro* and immunohistochemical identification of regenerated axons

Axonal regeneration was detected with a three-dimensional culture of adult rat DRG explants embedded in collagen gel as described previously.[27,49] During the experiment (for 7 days), either rmGal-1α or rmGal-1β was added to the culture system at a final concentration of 0.05, 0.5 and 5 ng/ml. For immunofluorescence microscopy, the tissues were fixed with 4% paraformaldehyde. An anti-βIII tubulin monoclonal antibody (Promega) was applied to the fixed tissues in 0.3% Triton X-100 in PBS for 2 days. A *FITC-labeled goat anti-mouse IgG antibody (Chemicon)* was applied for 2 days. The tissue was observed with a fluorescence microscope (Nikon TE 300) equipped with a color chilled 3CCD camera (Hamamatsu, C5810).

Acknowledgements

We extend our special thanks to Drs. S Hirano, M Furuichi, Y Tominaga, T Kadoya, S Kanba and Y Ohnishi for helpful discussions, and to Dr. B Quinn for useful comments on this manuscript.

References

1. Nakabeppu Y, Ryder K and Nathans D (1988) DNA binding activities of three murine Jun proteins: stimulation by Fos. Cell 55: 907–915
2. Chinenov Y and Kerppola TK (2001) Close encounters of many kinds: Fos–Jun interactions that mediate transcription regulatory specificity. Oncogene 20: 2438–2452
3. Jochum W, Passegué E and Wagner EF (2001) AP-1 in mouse development and tumorigenesis. Oncogene 20: 2401–2412
4. Shaulian E and Karin M (2001) AP-1 in cell proliferation and survival. Oncogene 20: 2390–2400
5. Nakabeppu Y and Nathans D (1991) A naturally occurring truncated form of FosB that inhibits Fos/Jun transcriptional activity. Cell 64: 751–759
6. Nishioka T, Sakumi K, Miura T, Tahara K, Horie H, Kadoya T and Nakabeppu Y (2002) FosB gene products trigger cell proliferation and morphological alteration with an increased expression of a novel processed form of galectin-1 in the rat 3Y1 embryo cell line. J. Biochem. (Tokyo) 131: 653–661
7. Tahara K, Tsuchimoto D, Tominaga Y, Asoh S, Ohta S, Kitagawa M, Horie H, Kadoya T and Nakabeppu Y (2003) DeltaFosB, but not FosB, induces delayed apoptosis independent of cell proliferation in the Rat1a embryo cell line. Cell Death Differ. 10: 496–507
8. Barondes SH, Castronovo V, Cooper DN, Cummings RD, Drickamer K, Feizi T, Gitt MA, Hirabayashi J, Hughes C, Kasai K, Leffler H, Liu F-T, Lotan R, Mercurio AM, Monsigny M, Pillai S, Poirier F, Raz A, Rigby PW, Rini JM and Wang JL (1994) Galectins: a family of animal beta-galactoside-binding lectins. Cell 76: 597–598
9. de Waard A, Hickman S and Kornfeld S (1976) Isolation and properties of beta-galactoside binding lectins of calf heart and lung. J. Biol. Chem. 251: 7581–7587
10. Poirier F, Timmons PM, Chan CT, Guénet JL and Rigby PW (1992) Expression of the L14 lectin during mouse embryogenesis suggests multiple roles during pre- and post-implantation development. Development 115: 143–155
11. Allen HJ, Gottstine S, Sharma A, DiCioccio RA, Swank RT and Li H (1991) Synthesis, isolation, and characterization of endogenous beta-galactoside-binding lectins in human leukocytes. Biochemistry 30: 8904–8910
12. Levi G and Teichberg VI (1984) The distribution of electrolectin in mouse: genetic and ontogenic variations. Biochem. Biophys. Res. Commun. 119: 801–806
13. Catt JW, Harrison FL and Carleton JS (1987) Distribution of an endogenous beta-galactoside-specific lectin during foetal and neonatal rabbit development. J. Cell. Sci. 87 (Part 5): 623–633
14. Powell JT (1980) Purification and properties of lung lectin. Rat lung and human lung beta-galactoside-binding proteins. Biochem. J. 187: 123–129
15. Hirabayashi J and Kasai K (1984) Human placenta beta-galactoside-binding lectin. Purification and some properties. Biochem. Biophys. Res. Commun. 122: 938–944
16. Allen HJ, Sucato D, Woynarowska B, Gottstine S, Sharma A and Bernacki RJ (1990) Role of galaptin in ovarian carcinoma adhesion to extracellular matrix *in vitro*. J. Cell. Biochem. 43: 43–57
17. Wells V and Mallucci L (1991) Identification of an autocrine negative growth factor: mouse beta-galactoside-binding protein is a cytostatic factor and cell growth regulator. Cell 64: 91–97
18. Perillo NL, Pace KE, Seilhamer JJ and Baum LG (1995) Apoptosis of T cells mediated by galectin-1. Nature 378: 736–739
19. Perillo NL, Uittenbogaart CH, Nguyen JT and Baum LG (1997) Galectin-1, an endogenous lectin produced by thymic epithelial cells, induces apoptosis of human thymocytes. J. Exp. Med. 185: 1851–1858
20. Paz A, Haklai R, Elad-Sfadia G, Ballan E and Kloog Y (2001) Galectin-1 binds oncogenic H-Ras to mediate Ras membrane anchorage and cell transformation. Oncogene 20: 7486–7493
21. Elad-Sfadia G, Haklai R, Ballan E, Gabius HJ and Kloog Y (2002) Galectin-1 augments Ras activation and diverts Ras signals to Raf-1 at the expense of phosphoinositide 3-kinase. J. Biol. Chem. 277: 37169–37175
22. Vyakarnam A, Lenneman AJ, Lakkides KM, Patterson RJ and Wang JL (1998) A comparative nuclear localization study of galectin-1 with other splicing components. Exp. Cell. Res. 242: 419–428
23. Park JW, Voss PG, Grabski S, Wang JL and Patterson RJ (2001) Association of galectin-1 and galectin-3 with Gemin4 in complexes containing the SMN protein. Nucleic Acids Res. 29: 3595–3602
24. Clerch LB, Whitney P, Hass M, Brew K, Miller T, Werner R and Massaro D (1988) Sequence of a full-length cDNA for rat lung beta-galactoside-binding protein: primary and secondary structure of the lectin. Biochemistry 27: 692–699
25. Liao DI, Kapadia G, Ahmed H, Vasta GR and Herzberg O (1994) Structure of S-lectin, a developmentally regulated vertebrate beta-galactoside-binding protein. Proc. Natl. Acad. Sci. USA 91: 1428–1432
26. Bourne Y, Bolgiano B, Nésa MP, Penfold P, Johnson D, Feizi T and Cambillau C (1994) Crystallization and preliminary X-ray diffraction studies of the soluble 14 kDa beta-galactoside-binding lectin from bovine heart. J. Mol. Biol. 235: 787–789
27. Horie H, Inagaki Y, Sohma Y, Nozawa R, Okawa K, Hasegawa M, Muramatsu N, Kawano H, Horie M, Koyama H, Sakai I, Takeshita K, Kowada Y, Takano M and Kadoya T (1999) Galectin-1 regulates initial axonal growth in peripheral nerves after axotomy. J. Neurosci. 19: 9964–9974
28. Horie H and Kadoya T (2000) Identification of oxidized galectin-1 as an initial repair regulatory factor after axotomy in peripheral nerves. Neurosci. Res. 38: 131–137
29. Inagaki Y, Sohma Y, Horie H, Nozawa R and Kadoya T (2000) Oxidized galectin-1 promotes axonal regeneration in peripheral nerves but does not possess lectin properties. Eur. J. Biochem. 267: 2955–2964

30. Cho M and Cummings RD (1996) Characterization of monomeric forms of galectin-1 generated by site-directed mutagenesis. Biochemistry 35: 13081–13088
31. Yang JT, Wu CS and Martinez HM (1986) Calculation of protein conformation from circular dichroism. Methods Enzymol. 130: 208–269
32. Johnson Jr WC (1990) Protein secondary structure and circular dichroism: a practical guide. Proteins 7: 205–214
33. Barondes SH, Cooper DN, Gitt MA and Leffler H (1994) Galectins. Structure and function of a large family of animal lectins. J. Biol. Chem. 269: 20807–20810
34. Lakowics JR (1999) Principles of Fluorescence Spectroscopy, 2nd ed. New York: Plenum publishers pp 456–458
35. Cho M and Cummings RD (1995) Galectin-1, a beta-galactoside-binding lectin in Chinese hamster ovary cells.I. Physical and chemical characterization. J. Biol. Chem. 270: 5198–5206
36. Fouillit M, Lévi-Strauss M, Giudicelli V, Lutomski D, Bladier D, Caron M and Joubert-Caron R (1998) Affinity purification and characterization of recombinant human galectin-1. J. Chromatogr. B Biomed. Sci. Appl. 706: 167–171
37. Walzel H, Schulz U, Neels P and Brock J (1999) Galectin-1, a natural ligand for the receptor-type protein tyrosine phosphatase CD45. Immunol. Lett. 67: 193–202
38. Fajka-Boja R, Szemes M, Ion G, Légrádi A, Caron M and Monostori E (2002) Receptor tyrosine phosphatase, CD45 binds galectin-1 but does not mediate its apoptotic signal in T cell lines. Immunol. Lett. 82: 149–154
39. Giudicelli V, Lutomski D, Lévi-Strauss M, Bladier D, Joubert-Caron R and Caron M (1997) Is human galectin-1 activity modulated by monomer/dimer equilibrium? Glycobiology 7 viii–x
40. Tracey BM, Feizi T, Abbott WM, Carruthers RA, Green BN and Lawson AM (1992) Subunit molecular mass assignment of 14,654 Da to the soluble beta-galactoside-binding lectin from bovine heart muscle and demonstration of intramolecular disulfide bonding associated with oxidative inactivation. J. Biol. Chem. 267: 10342–10347
41. Imbe H, Okamoto K, Kadoya T, Horie H and Senba E (2003) Galectin-1 is involved in the potentiation of neuropathic pain in the dorsal horn. Brain Res. 993: 72–83
42. Horie H, Kadoya T, Hikawa N, Sango K, Inoue H, Takeshita K, Asawa R, Hiroi T, Sato M, Yoshioka T and Ishikawa Y (2004) Oxidized galectin-1 stimulates macrophages to promote axonal regeneration in peripheral nerves after axotomy. J. Neurosci. 24: 1873–1880
43. McGahan L, Hakim AM, Nakabeppu Y and Robertson GS (1998) Ischemia-induced CA1 neuronal death is preceded by elevated FosB and Jun expression and reduced NGFI-A and JunB levels. Brain Res. Mol. Brain Res. 56: 146–161
44. Hope BT, Nye HE, Kelz MB, Self DW, Iadarola MJ, Nakabeppu Y, Duman RS and Nestler EJ (1994) Induction of a long-lasting AP-1 complex composed of altered Fos-like proteins in brain by chronic cocaine and other chronic treatments. Neuron 13: 1235–1244
45. Chen J, Nye HE, Kelz MB, Hiroi N, Nakabeppu Y, Hope BT and Nestler EJ (1995) Regulation of delta FosB and FosB-like proteins by electroconvulsive seizure and cocaine treatments. Mol. Pharmacol. 48: 880–889
46. Hirano S, Tominaga Y, Ichinoe A, Ushijima Y, Tsuchimoto D, Honda-Ohnishi Y, Ohtsubo T, Sakumi K and Nakabeppu Y (2003) Mutator phenotype of MUTYH-null mouse embryonic stem cells. J. Biol. Chem. 278: 38121–38124
47. Studier FW, Rosenberg AH, Dunn JJ and Dubendorff JW (1990) Use of T7 RNA polymerase to direct expression of cloned genes. Methods Enzymol. 185: 60–89
48. Bladier D, Joubert R, Avellana-Adalid V, Kemeny JL, Doinel C, Amouroux J and Caron M (1989) Purification and characterization of a galactoside-binding lectin from human brain. Arch. Biochem. Biophys. 269: 433–439
49. Horie H, Sakai I, Akahori Y and Kadoya T (1997) IL-1 beta enhances neurite regeneration from transected-nerve terminals of adult rat DRG. NeuroReport 8: 1955–1959
50. Martz E (2002) Protein explorer: easy yet powerful macromolecular visualization. Trends Biochem. Sci. 27: 107–109

Cell Death and Differentiation (2005), 1–13

www.nature.com/cdd

MTH1, an oxidized purine nucleoside triphosphatase, protects the dopamine neurons from oxidative damage in nucleic acids caused by 1-methyl-4-phenyl-1,2,3,6-tetrahydropyridine

H Yamaguchi[1], K Kajitani[1], Y Dan[1], M Furuichi[2], M Ohno[1], K Sakumi[1], D Kang[3] and Y Nakabeppu*,[1]

[1] Division of Neurofunctional Genomics, Department of Immunobiology and Neuroscience, Medical Institute of Bioregulation, Kyushu University, Fukuoka 812-8582, Japan
[2] Radioisotope center, Kyushu University, Fukuoka 812-8582, Japan
[3] Department of Clinical Chemistry and Laboratory Medicine, Graduate School of Medical Sciences, Kyushu University, Fukuoka 812-8582, Japan
* Corresponding author: Y Nakabeppu, Division of Neurofunctional Genomics, Department of Immunobiology and Neuroscience, Medical Institute of Bioregulation, Kyushu University, 3-1-1 Maidashi Higashi-ku, Fukuoka, 812-8582, Japan. Tel: +81 92 642 6800; Fax: +81 92 642 6791; E-mail: yusaku@bioreg.kyushu-u.ac.jp

Received 17.6.05; revised 30.8.05; accepted 30.8.05
Edited by H Ichijo

Abstract

We previously reported that 8-oxoguanine (8-oxoG) accumulates in the cytoplasm of dopamine neurons in the substantia nigra of patients with Parkinson's disease and the expression of MTH1 carrying an oxidized purine nucleoside triphosphatase activity increases in these neurons, thus suggesting that oxidative damage in nucleic acids is involved in dopamine neuron loss. In the present study, we found that levels of 8-oxoG in cellular DNA and RNA increased in the mouse nigrostriatal system during the tyrosine hydroxylase (TH)-positive dopamine neuron loss induced by the administration of 1-methyl-4-phenyl-1,2,3,6-tetrahydropyridine (MPTP). MTH1-null mice exhibited a greater accumulation of 8-oxoG in mitochondrial DNA accompanied by a more significant decrease in TH and dopamine transporter immunoreactivities in the striatum after MPTP administration, than in wild-type mice. We thus demonstrated that MTH1 protects the dopamine neurons from oxidative damage in the nucleic acids, especially in the mitochondrial DNA of striatal nerve terminals of dopamine neurons.
Cell Death and Differentiation advance online publication, 4 November 2005; doi:10.1038/sj.cdd.4401788

Keywords: MPTP; 8-oxoguanine; Parkinson's disease; mitochondria; striatum

Abbreviations: 2-OH-dATP, 2-hydroxy-2′-deoxyadenosine triphosphate; 8-oxo-dGTP, 8-oxo-2′-deoxyguanosine triphosphate; 8-oxo-dG, 8-oxo-2′-deoxyguanosine; 8-oxoG, 8-oxoguanine; AD, Alzheimer's disease; DAT, dopamine transporter; dG, 2′-deoxyguanosine; GFAP, glial fibrillary acidic protein; mAb, monoclonal antibody; MPP^+, 1-methyl-4-phenylpryridinium; MPTP, 1-methyl-4-phenyl-1,2,3,6-tetrahydropyridine; NAc, nucleus accumbens; OT, olfactory tubercle; PD, Parkinson's disease; SN, substantia nigra; SNc, substantia nigra pars compacta; SNr, substantia nigra pars reticulata; TH, tyrosine hydroxylase; VTA, ventral tegmental area; VDAC, voltage-dependent anion-selective channel

Introduction

The accumulation of oxidative damage in cellular DNA or RNA, which is one of major causes for mutagenesis and cell death during aging, is a result of the incorporation of the oxidized nucleotides generated in nucleotide pools as well as a result of their direct oxidation.[1] To minimize the incorporation of oxidized nucleotides into cellular DNA or RNA, organisms normally come equipped with an elaborate mechanism to sanitize the nucleotides pools. In *Escherichia coli,* MutT hydrolyzes 8-oxo-2′-deoxyguanosine triphosphate (8-oxo-dGTP) and 8-oxo-GTP to monophosphate forms thereby avoiding the misincorporation of such mutagenic nucleotides into DNA or mRNA.[2] We identified MutT homologues in human and rodent cells and they were found to suppress the elevated spontaneous mutation rates of *mutT* mutants to an almost normal level, and they were thus designated as MTH1 (MutT homolog-1).[2,3] MTH1, but not *E. coli* MutT, has an ability to efficiently hydrolyze oxidized dATP and ATP, such as 2-hydroxy-2′-deoxyadenosine triphosphate (2-OH-dATP), and 2-OH-ATP, as well as 8-oxo-dGTP or 8-oxoGTP, and thus designated MTH1 as an oxidized purine nucleoside triphosphatase.[3,4]

It has been established that oxidative DNA damage, such as 8-oxoguanine (8-oxoG), accumulates both in nuclear and mitochondrial genomes during aging,[5,6] and such accumulation is likely to increase dramatically in patients with tumors[7] or various neurodegenerative diseases, such as Parkinson's disease (PD),[8,9] Alzheimer's disease (AD)[10] or amyotrophic lateral sclerosis.[11] We have shown that a significant increase of 8-oxoG accumulated in the cytoplasm or mitochondria with a coincidentally elevated expression of MTH1 in the substantia nigral neurons of PD patients.[9] In postmortem tissue specimens from patients with AD, the expression levels of MTH1 in the entorhinal cortex were also elevated, while the levels of MTH1 apparently decreased in the stratum lucidum at CA3 corresponding to the mossy fiber synapses, where MTH1 is highly expressed in control subjects.[12] These observations strongly suggest that MTH1 plays an important role in protecting neurons from oxidative damage.

To characterize the biological importance of MTH1, we established MTH1-null mice and found them to exhibit an increased occurrence of spontaneous carcinogenesis especially in the liver, and to a lesser extent in the lung and

stomach.[13] We recently reported that MTH1-null fibroblasts were highly susceptible to cell dysfunction and death caused by exposure to H_2O_2, with morphological features of pyknosis and electron dense deposits accumulated in the mitochondria, accompanied by a continuous accumulation of 8-oxoG both in nuclear and mitochondrial DNA.[14] All of the H_2O_2-induced alterations observed in MTH1-null fibroblasts were effectively suppressed by the expression of wild-type human MTH1, thus demonstrating that MTH1 indeed protects cells from oxidative damage.

In the present study, we show that the levels of 8-oxoG in cellular DNA and RNA increased in the mouse nigrostriatal system during the dopamine neuron loss induced by the systemic administration of 1-methyl-4-phenyl-1,2,3,6-tetrahydropyridine (MPTP). Moreover, MTH1-null mice exhibited an increased accumulation of 8-oxoG in mitochondrial DNA in the striatum followed by a more significant neuronal dysfunction after MPTP administration, in comparison to wild type.

Results

Spontaneous oxidative damage in nucleic acids of normal mouse brain

To evaluate the spontaneous levels and distributions of the oxidative damage of nucleic acids in normal mouse brain, the levels of 8-oxoG in cellular DNA and RNA were analyzed. Brain sections were subjected to immunohistochemistry with two different monoclonal antibodies (mAbs) which preferentially react with either 8-oxoG in DNA (N45.1) or RNA (15A3) using proper pretreatments.

In samples pretreated with RNase and HCl, the N45.1 mAb exhibited nuclear immunoreactivities mostly in neurons throughout the brain including the hippocampus (Figure 1Aa, c) and substantia nigra (SN) (Figure 1Ab, d). These immunoreactivities were abolished by either the pretreatment of the sections with DNase (Figure 1Ae, f) or the preadsorption of the antibody with 8-oxo-dG (Figure 1Ag, h) but not 2′-deoxyguanosine (dG) (Figure 1Ai, j), thus indicating that guanine residues in the nuclear DNA of neurons are spontaneously oxidized to some extent. We also measured the 8-oxoG levels in nuclear DNA prepared from various regions of mouse brain by HPLC–MS/MS method (Table 1). About 2.5–3 residues of 8-oxoG per 10^6 guanine residues were present in the nuclear DNA from the cerebrum, cerebellum, other brain region that contains striatum, thalamus and brainstem, and the liver from control wild-type and MTH1-null mice.

In samples without any pretreatment, in contrast, the 15A3 mAb exhibited cytoplasmic immunoreactivities in the whole brain region including the cerebral cortex, hippocampus (Figure 1Ba, c) and SN (Figure 1Bb, d), and again these immunoreactivities were abolished by either the pretreatment of sections with RNase (Figure 1Be, f) or the preadsorption of the antibody with 8-oxo-dG (Figure 1Bg, h) but not dG (Figure 1Bi, j). These results indicate that there are substantial levels of spontaneously oxidized guanine in cellular RNA.

In samples pretreated only with RNase, the N45.1 mAb exhibited weak cytoplasmic or perinuclear immunoreactivities in the neurons (Figure 1C), and these immunoreactivities were mostly merged with immunoreactivities to antibodies against the mitochondrial protein, voltage-dependent anion-selective channel (VDAC) (Figure 1Cc, d). These findings indicate that guanine residues in the mitochondrial DNA in neurons are also spontaneously oxidized.

Systemic administration of MPTP caused accumulation of 8-oxoG in cellular DNA and RNA in dopamine neurons in the nigrostriatal system

We and others have shown that the 8-oxoG content in cellular DNA and RNA significantly increased in SN neurons in patients with PD.[8,9] To address whether the levels of oxidative damage of nucleic acids in the neurons increase during dopamine neuron loss, we focused on the MPTP-induced PD mouse model.

Mice were injected intraperitoneally (i.p.) with MPTP (30 mg/kg), and then were killed 6, 12, 24 h after the injection, or 54 h after the first injection with three consecutive injections every 24 h (Figure 2A). at 6 h after MPTP injection, neither a decrease of tyrosine hydroxylase (TH) immunoreactivitiy, which is a phenotypic marker for dopamine neurons, nor an increase of 8-oxoG immunoreactivities in RNA and DNA was seen in the SN (data not shown). At 12 h after MPTP injection, a decrease of TH immunoreactivitiy was not seen yet (Figure 2Ba, b), however, an increased microglial activation, characterized by an amoeboid morphology with an increase in the expression of the CD11b detected by Mac-1 antibody, was observed in the SN pars compacta (SNc) (Figure 2Be, f). Thereafter, 8-oxoG immunoreactivitiy both in DNA and RNA in SN apparently increased (Figure 2Bi–l, m–p). At 24 h after the first MPTP injection, a decrease of TH immunoreactivitiy, thus indicating dopamine neuron loss, was still not apparent (Figure 2Bc), however, 54 h later after three MPTP injections, the loss became highly prominent (Figure 2Bd), and accompanied with more activated microglias (Figure 2Bg, h).

To compare the extent of 8-oxoG accumulation in RNA in neurons in the SNc and SN pars reticulata (SNr) after MPTP injection, the immunoreactivities for 8-oxoG in each region were separately digitized from the data shown in Figure 2B (m–p), and the level of 8-oxoG in each sample was determined. At 12 h after the first MPTP injection, the contents of 8-oxoG in the cellular RNA both in the SNc and SNr increased to about 140–150% of the levels seen in the control, and thereafter gradually decreased following the second and third injections (Figure 2C).

In order to confirm that the 8-oxoG immunoreactivities increased in dopamine neurons in the SN, we performed double-immunofluorescence microscopy using anti-TH and anti-8-oxoG (15A3). The increase of 8-oxoG immunoreactivitiy in RNA 12 h after MPTP injection was apparently observed in most of the TH-positive dopamine neurons in the SNc (Figure 3A).

The 8-oxoG immunoreactivitiy in the nuclear DNA of TH-positive dopamine neurons in the SNc was determined by laser scanning confocal microscopy. In the control, 8-oxoG immunoreactivitiy in the nuclei of TH-positive neurons was apparently lower than that in the nuclei of the surrounding

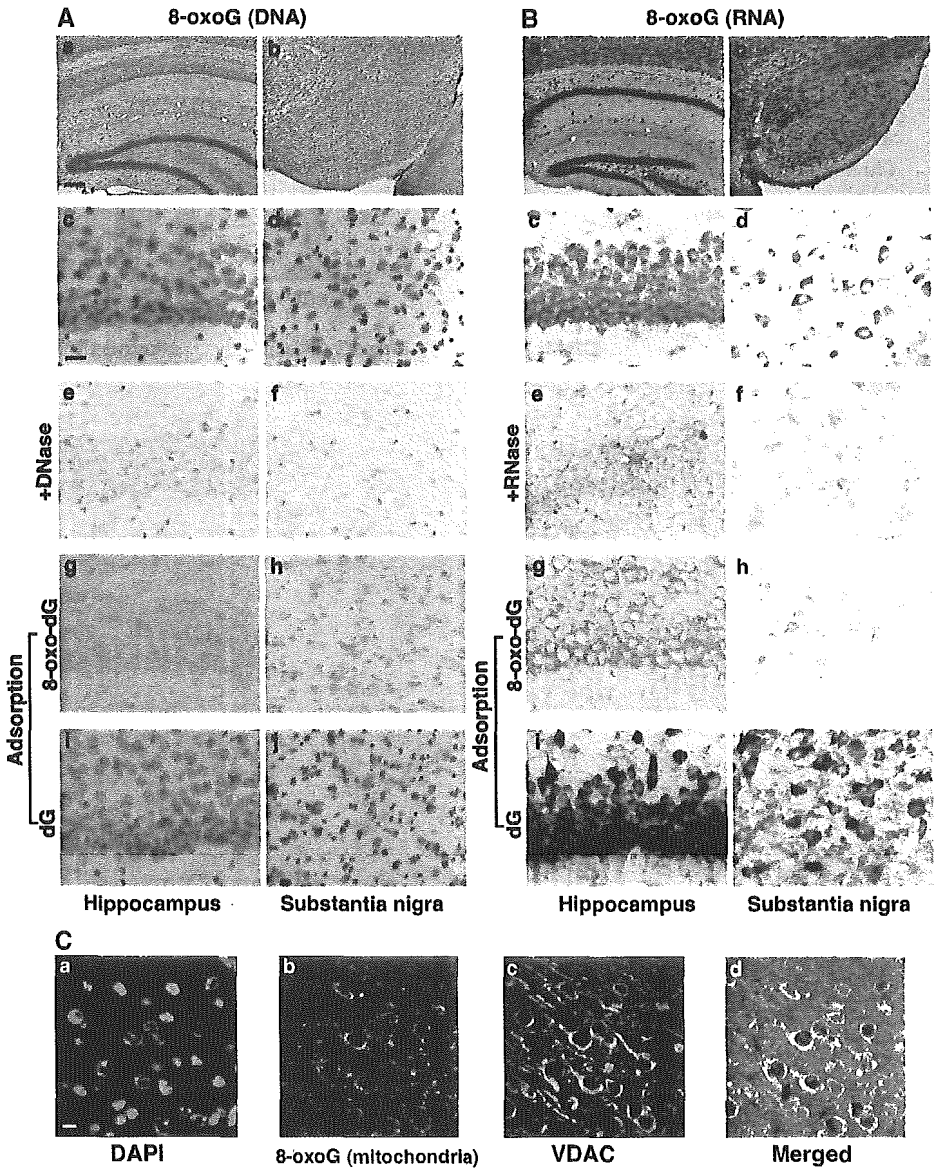

Figure 1 Spontaneous oxidative damage in nucleic acids of normal mouse brain. (**A**) Detection of 8-oxoG in cellular DNA. The sections prepared from 10-week-old C57BL/6J male mice were subjected to immunohistochemistry with the N45.1 mAb after RNase and HCl treatment. The sections pretreated with DNase (e, f) exhibited little reactivity with the antibody, and preadsorption of the antibody with 8-oxo-dG (g, h) but not with dG (i, j) abolished the immunoreactivitiy. Hippocampus (a, c, e, g, i), SN (b, d, f, h, j). Scale bars: a–b, 200 μm; c–j, 20 μm. (**B**) Detection of 8-oxo-G in cellular RNA. The sections were subjected to immunohistochemistry with the 15A3 mAb without pretreatment. Cytoplasmic immunoreactivities were observed mostly in the neurons of hippocampus (a, c) and SN (b, d). The sections pretreated with RNase (e, f) exhibited little reactivity with the antibody, and preadsorption of the antibody with 8-oxo-dG (g, h) but not with dG (i, j) abolished the immunoreactivitiy. (**C**) Detection of 8-oxoG in the mitochondrial DNA. The sections were subjected to immunohistochemistry with the N45.1 mAb after RNase treatment. Laser-scanned confocal images from the cerebral cortex stained for nuclear DNA with DAPI (a), 8-oxoG (b), VDAC (c), and merged image (d) were shown. Weak perinuclear immunoreactivities for 8-oxoG were observed in large neurons (b), and these immunoreactivities were mostly merged with the mitochondrial protein VDAC immunoreactivitiy (c, d). Scale bar: 10 μm

TH-negative cells (Figure 3Ba), while the nuclear immunoreactivitiy in the TH-positive neurons significantly increased 54 h after MPTP administration (Figure 3Bb). The fluorescence intensity for 8-oxoG immunoreactivitiy was digitized and the level of 8-oxoG in each sample was determined (Figure 3C). The content of 8-oxoG in the nuclear DNA in the TH-positive neurons in the SNc increased gradually to the 140% level seen in the control during the 24 h period after the first MPTP injection, and thereafter gradually decreased following the second and third injections.

We next examined the extent of TH, CD11b, glial fibrillary acidic protein (GFAP) and 8-oxoG immunoreactivities in the striatum after MPTP administration. At 12 h after MPTP injection, a decrease in TH immunoreactivitiy indicating terminal dysfunction of dopamine neurons was apparent (Figure 4B), and an increased microglial activation was also

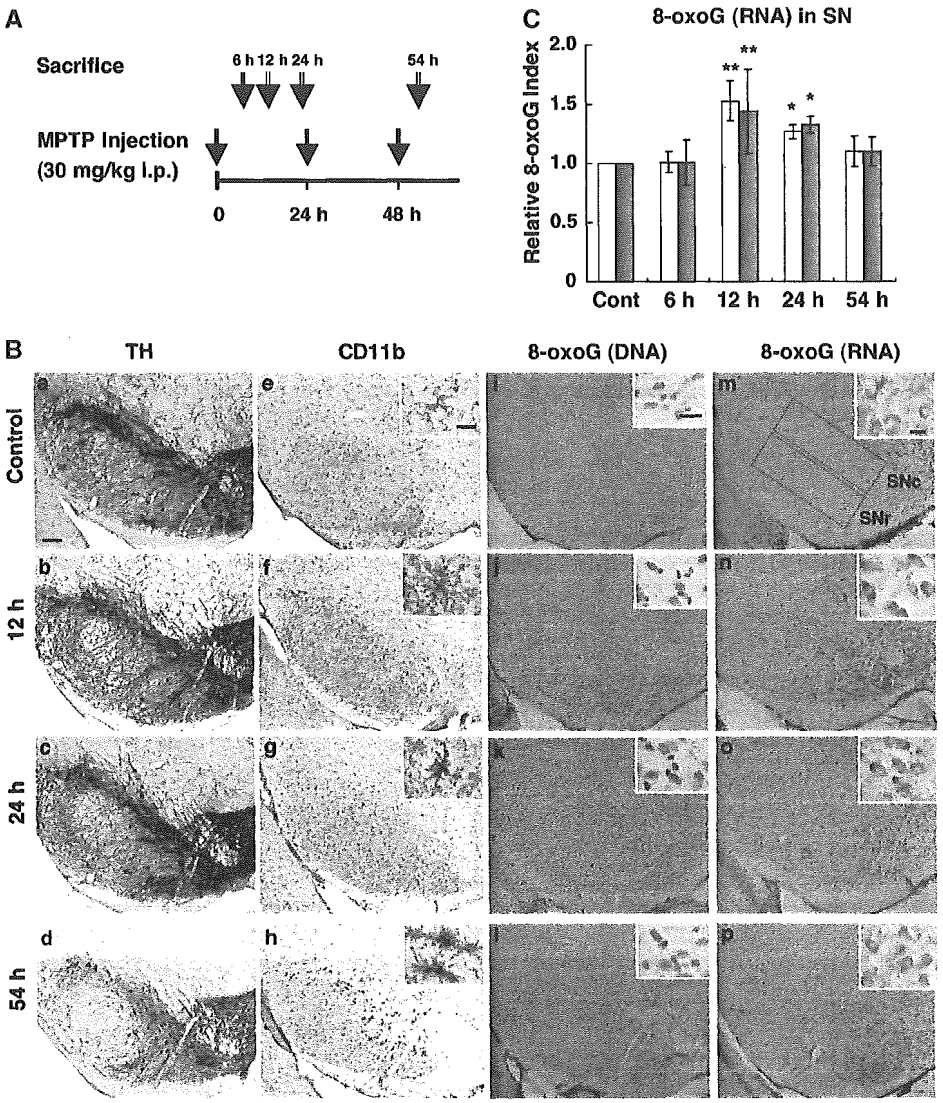

Figure 2 Systemic administration of MPTP increased the accumulation of 8-oxoG in nuclear DNA and cellular RNA of dopamine neurons in the substantia nigra prior to their loss. (**A**) 10-week-old C57BL/6J male mice ($n=4$ per group) were injected i.p with MPTP (30 mg/kg). The mice received a single injection of MPTP were killed 6, 12, 24 h after the injection, and those received three injections of MPTP were killed 54 h after the first injection. (**B**) Immunohistochemical detection of TH (a–d), CD11b (e–h), 8-oxoG in DNA (i–l) and 8-oxoG in RNA (m–p). Control mice (a, e, i, m); 12 h after the first MPTP injection (b, f, j, n); 24 h after the first injection (c, g, k, o); 54 h after the first injection with three injections of MPTP (d, h, l, p). Insets in panels (e–p) indicate enlarged view of each section. Scale bars (a–p), 200 μm; inset, 20 μm. (**C**) The increased accumulation of 8-oxoG in cellular RNA in the SN after MPTP administration. Immunoreactivities for 8-oxoG in SNc (open bars) and SNr (gray bars), as shown in Figure 2Bm, were separately digitized from the data shown in Figure 2B(m–p), and 8-oxoG index in each sample was determined. The relative value of each 8-oxoG index to that of the control is shown as a bar graph with the means $\pm$ S.D ($n=4$ per group). Mann–Whitney *U*-test, $^{**}P<0.01$, $^{*}P<0.05$ compared to the control

Table 1 The contents of 8-oxoG in nuclear DNA prepared from parts of the brains and livers from the control mice and MPTP-treated mice

	8-OxoG per 10^6 guanine residues			
	Control		MPTP	
Tissues	**Wild type**	**MTH1-null**	**Wild type**	**MTH1-null**
Cerebrum	2.54±0.37	2.42±0.28	3.36±0.23	3.42±0.11
Cerebellum	2.76±0.10	2.27±0.19	2.99±0.16	3.17±0.11
Other brain region	2.79±0.19	3.11±0.37	3.32±0.22	3.99±0.44
Liver	3.02±0.09	2.85±0.13	3.02±0.26	2.85±0.31

MPTP (30 mg/kg) or saline (control) was administered i.p to wild-type and MTH1-null mice once a day for 5 consecutive days. At 7 days after the last injection, the mice were killed for analyses. Number of mice was five for each group except MTH1-null control ($N=4$). Nuclear DNA isolated from the tissues were analyzed by HPLC–MS/MS to determine the contents of 8-oxoG. Data indicated are the mean±S.E.M. There is no significant difference in 8-oxoG levels between wild-type and MTH1-null mice (Mann–Whitney *U*-test, $P>0.05$).